

# **Effect of strain path on the evolution of microstructure and texture of equiatomic CoCrFeMnNi high entropy alloy**

Seelam Rajasekhar Reddy

A Dissertation Submitted to  
Indian Institute of Technology Hyderabad  
In Partial Fulfillment of the Requirements for  
The Degree of Master of Technology



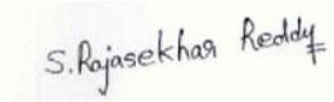
भारतीय प्रौद्योगिकी संस्थान हैदराबाद  
Indian Institute of Technology Hyderabad

Department of Materials Science and Metallurgical Engineering

June, 2016

## Declaration

I declare that this written submission represents my ideas in my own words, and where others' ideas or words have been included, I have adequately cited and referenced the original sources. I also declare that I have adhered to all principles of academic honesty and integrity and have not misrepresented or fabricated or falsified any idea/data/fact/source in my submission. I understand that any violation of the above will be a cause for disciplinary action by the Institute and can also evoke penal action from the sources that have thus not been properly cited, or from whom proper permission has not been taken when needed.



S. Rajasekhar Reddy

---

(Signature)

---

Seelam Rajasekhar Reddy

(– Student Name –)

---

MS14M16P000001

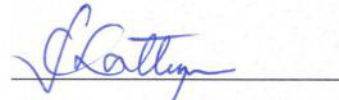
(Roll No)

## Approval Sheet

This thesis entitled “**Effect of strain path on the evolution of microstructure and texture of equiatomic CoCrFeMnNi high entropy alloy**” by Seelam Rajasekhar Reddy is approved for the degree of Master of Technology from IIT Hyderabad.



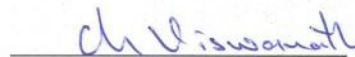
Dr. Saswata Bhattacharya  
Department of Materials Science and Metallurgical Engineering  
Examiner



Dr. Subhradeep Chatterjee  
Department of Materials Science and Metallurgical Engineering  
Examiner



Dr. Pinaki Prasad Bhattacharjee  
Department of Materials Science and Metallurgical Engineering  
Adviser



Dr. Chinthapenta R Viswanath  
Department of Mechanical and Aerospace Engineering  
Chairman

## Acknowledgements

First and foremost, I would like to express my heartfelt and sincerest thanks to my thesis supervisor **Dr. Pinaki Prasad Bhattacharjee**, for his esteemed guidance and consistent encouragement throughout my research work. This work would not have been possible without his assistance and endless patience throughout the course of time.

I would like to thank Prof. J. W. Yeh, from Materials Science and Engineering, National Tsing Hua University, Taiwan for providing the starting material for our work.

I would like to thank Dr. Zaid Ahmed and Dr. Dan Sathiaraj for extending their constant support at any point of time, right from experiments stage till analysis of the results.

I would like to thank all the faculty members, research scholars and technical staff for extending their help and support.

Finally, I would like to thank all my friends and beloved family members for their love and support over the past two years and making this short time a memorable experience.

Dedicated to

**My Parents**

## Abstract

The effect of strain path on the evolution of microstructure and texture during cold rolling and subsequent annealing was investigated in equiatomic CoCrFeMnNi high entropy alloy. For this purpose the alloy was subjected to cold rolling up to 90% reduction in thickness by four different strain path routes namely (i) unidirectional rolling (UCR); (ii) Multi step cross rolling (MSCR); (iii) two step cross rolling (90°) (TSCR [90°]); (iv) two step cross rolling (45°) (TSCR [45°]). These deformed samples were subjected to isochronal annealing (for 1 h) at different temperatures ranging from 700°C to 1000°C and were characterized by using electron backscattered diffraction (EBSD) technique. Development of ultrafine microstructure and presence of shear bands in all deformed materials attributes to the grain subdivision at finer scale. The differently cross rolled materials shown weaker brass and stronger ND rotated brass components in contrast to UCR processed material where strong brass type texture was observed. The cross rolled materials showed significant coarse grain size compared to UCR with fine grain size reveals the lesser density of potential nucleation sites due to the destabilization of substructure as a result of the change in strain path. TSCR (45°) processed material showed further increase in grain size which appeared to be due to the propagation of intersecting shear bands which further destroys nucleation environment. The recrystallization texture of all the processed materials showed presence of  $\alpha$  fiber and retention of deformation texture components which could be explained on the basis of the absence of strong preferential nucleation and growth.

# Nomenclature

HEA- High Entropy Alloy

TMP- Thermo-mechanical processing

FCC- Face Centered Cubic

BCC- Body Centered Cubic

GB map- Grain Boundary map

IQ map- Image Quality map

ODF- Orientation Distribution Function

PF- Pole Figure

RD- Rolling Direction

TD- Transverse Direction

ND- Normal Direction

UCR-Unidirectional Rolling

MSCR-Multi Step Cross Rolling

TSCR (90°)-Two Step Cross Rolling (90°)

TSCR (45°)-Two Step Cross Rolling (45°)

SFE- Stacking Fault Energy

DSS-Duplex stainless steel

HAB/HAGB- High Angle Grain Boundary

TB- Twin Boundary

EBSD- Electron Back Scattered Diffraction

B<sub>S</sub> - Brass orientation

B<sub>S</sub><sup>ND</sup> - ND rotated Brass orientation

BR- Recrystallized Brass orientation

G- Goss orientation

Rt G - Rotated Goss orientation

# Contents

Declaration.....	ii
Approval Sheet .....	iii
Acknowledgements .....	iv
Abstract.....	vi
<b>Nomenclature .....</b>	<b>vii</b>
<b>1 Introduction.....</b>	<b>1</b>
1.1 Overview .....	1
1.2 Objective of present work.....	1
<b>2 Literature Review .....</b>	<b>2</b>
2.1 Thermomechanical processing of CoCrFeMnNi HEA .....	2
2.2 Effect of strain path on microstructure and texture formation .....	2
2.3 Novelty of the work .....	3
<b>3 Experimental methods.....</b>	<b>4</b>
3.1 Preparation of starting material .....	4
3.2 Processing.....	5
3.2.1 Cold rolling .....	5
3.2.2 Annealing.....	6
3.3 Material Charecterization .....	6
<b>4 Results.....</b>	<b>7</b>
4.1 Starting material .....	7
4.2 Deformation microstructure and texture.....	8
4.3 Microstructure and texture evolution of isochronal annealing.....	14
<b>5 Discussion .....</b>	<b>22</b>
5.1 Evolution of deformation microstructure and texture .....	22
5.2 Evolution of annealed microstructure and texture.....	24
<b>6 Summary and Conclusions .....</b>	<b>27</b>
<b>References.....</b>	<b>29</b>



# Chapter 1: Introduction

## 1.1 Overview

The conventional alloy design concept is based on one/two principal elements to which other alloying elements are added to enhance the properties. In sharp contrast to this established philosophy, recently a novel multi-component alloy design concept has been introduced based on mixing of a large number of elements ( $\geq 5$ ) in equiatomic or near equiatomic proportion [1]. Despite the presence of a large number of elements, the HEAs can show simple FCC, BCC or FCC+BCC structures [1, 2]. This is attributed to due to their high configurational entropy of mixing which reduces the free energy and stabilizes simple phases. The HEAs can show remarkable properties including high temperature structural stability [3], fracture resistance at cryogenic temperature [4], damage tolerance, formation of nano-crystalline structures [5], high wear resistance and excellent formability [6-10]. High entropy, sluggish diffusion, severe lattice distortion and cocktail effects [3, 5, 7, 10] have been identified as the core effects which significantly affect the development of microstructure and properties of HEAs.

Thermo-mechanical processing (TMP) can further enhance the properties of the HEAs by modifying the microstructure and crystallographic texture [11]. The effect of different parameters including cold-rolling strain [12], starting grain size [13], cryo-rolling [14] and heating rate [15] on the development of microstructure and texture during TMP of FCC equiatomic CoCrFeMnNi has been reported.

## 1.2 Objective of the present work

The present work attempts to understand the effect of strain path on the evolution of microstructure and texture during thermo-mechanical processing of equiatomic FCC HEA CoCrFeMnNi, which has not been reported as yet. For this purpose, four different rolling routes would be investigated. The microstructure and texture evolution during deformation and annealing would be investigated using electron backscatter diffraction (EBSD) technique.

## Chapter 2: Literature Review

### 2.1 Thermo-mechanical processing of CoCrFeMnNi HEA

Thermo-mechanical processing (TMP) of materials [16, 17] is a combination of deformation (such as rolling, forging or extrusion) and thermal treatments which in turn greatly affect the development of microstructure, texture and mechanical properties of the processed materials. TMP has been remarkably successful in refining the microstructure and achieving desired mechanical properties in a wide variety of materials including different alloys or even intermetallics. Therefore, unearthing the effect of different TMP parameters on microstructure, texture and mechanical properties of HEAs is of prime interest.

The quinary FCC CoCrFeMnNi has been extensively investigated as a model system to understand the TMP behavior of HEAs by Sathiaraj et al. [11-15]. The effect of cold-rolling strain, starting grain size, cryo-rolling has been systematically investigated by these authors. It has been clarified that the different TMP parameters greatly affect the deformation and recrystallization microstructures, however the development of texture is not greatly affected. The deformation texture of the quinary alloy is found to be of brass or alloy type, indicating the low SFE of this alloy. After recrystallization of the alloy, development of  $\alpha$ -fiber components and retention of deformation texture components such as S ( $\{123\}\langle 634\rangle$ ). However, the typical recrystallization component of low SFE brass i.e. the BR ( $\{236\}\langle 385\rangle$ ) and D components are found to be rather weak in the recrystallization texture of the quinary HEA. The distinctly different behavior of the HEA with the recrystallization texture of other low SFE alloys have been explained on the basis of absence of preferential nucleation and growth.

Another processing parameter which can greatly affect the development of microstructure and texture in different alloys is the strain path. Although the effect of change in strain path has been investigated in different alloys, this is yet to be investigated in the HEAs. This essentially remains the major objective of the present work.

### 2.2 Effect of strain path on microstructure and texture formation

The effect of strain path change under rolling deformation has been mostly investigated using different cross-rolling routes. During cross-rolling the rolling and transverse directions (RD and

TD, respectively) are mutually interchanged in each subsequent passes by rotating the sheet about the ND by 90°.

The deformation texture of heavily cold-rolled medium to high SFE alloys is described as pure metal or copper type due to the presence of stronger copper (Cu) ( $\{112\}\langle 111\rangle$ ) and S ( $\{123\}\langle 634\rangle$ ) as compared to the brass ( $B_S$ ) ( $\{110\}\langle 112\rangle$ ) component. In contrast, low SFE alloys develop a typical brass/alloy type deformation texture with strong  $B_S$  component. However, irrespective of the SFE, cross-rolling leads to significant strengthening of the  $B_S$  and ND-rotated Brass ( $B_S^{ND}$ ) components [18, 19]. Cross-rolling of Copper [18-21], Nickel [20, 22], Al [23], Stainless steel [18] and Duplex stainless steel (DSS) [24] show dominated  $B_S$  ( $\{110\}\langle 112\rangle$ ) and  $B_S^{ND}$   $\{110\}\langle 1-11\rangle$  components.

Upon recrystallization, the heavily cross-rolled medium to low SFE FCC materials do not show the usual cube component ( $\{001\}\langle 100\rangle$ ). In contrast, cross-rolled materials show rather weak cube texture after annealing. Development of unusual texture, such as  $\{111\}$  fiber has been reported in heavily cross-rolled Ni after recrystallization [25]. The recrystallization texture of cross-rolled low SFE materials is much less investigated. Retention of deformation texture components in the austenite of duplex steels has been observed, which has been attributed to the discontinuous recrystallization without preferential orientation selection.

### **2.3 Novelty of the work**

The present work investigates for the first time the effect of change in strain path during cold-rolling on the evolution of microstructure and texture in FCC equiatomic CoCrFeMnNi HEA. In order to achieve these objectives, the present work employs novel cross-rolling routes in addition to common cross-rolling techniques. It is envisaged that the present results will also be important for understanding the microstructure and texture development in other HEAs.

## Chapter 3: Experimental Methods

### 3.1 Preparation of starting material

As already stated FCC equiatomic CoCrFeMnNi was used. The equiatomic HEA was vacuum arc-melted from pure elements (with purity >99.9%) and cast into a slab with dimensions 10mm\*20mm\*40mm. Rectangular samples with dimensions 10mm\*20mm\*5mm were cut from the as-cast slab. These samples were homogenized at 1100°C for 6 hours (h) to attain chemical homogeneity. In order to break down the cast structure, the homogenized samples were cold-rolled to 50% reduction in thickness using a laboratory scale rolling equipment having roll diameter of ~ 140 mm (SPX Precision Instruments, Fenn Division, USA). The rolled samples were fully annealed at 800°C for 1 h and used as the starting material for further TMP. The schematic representation of the present work in the form of flow chart in Fig.3.1.

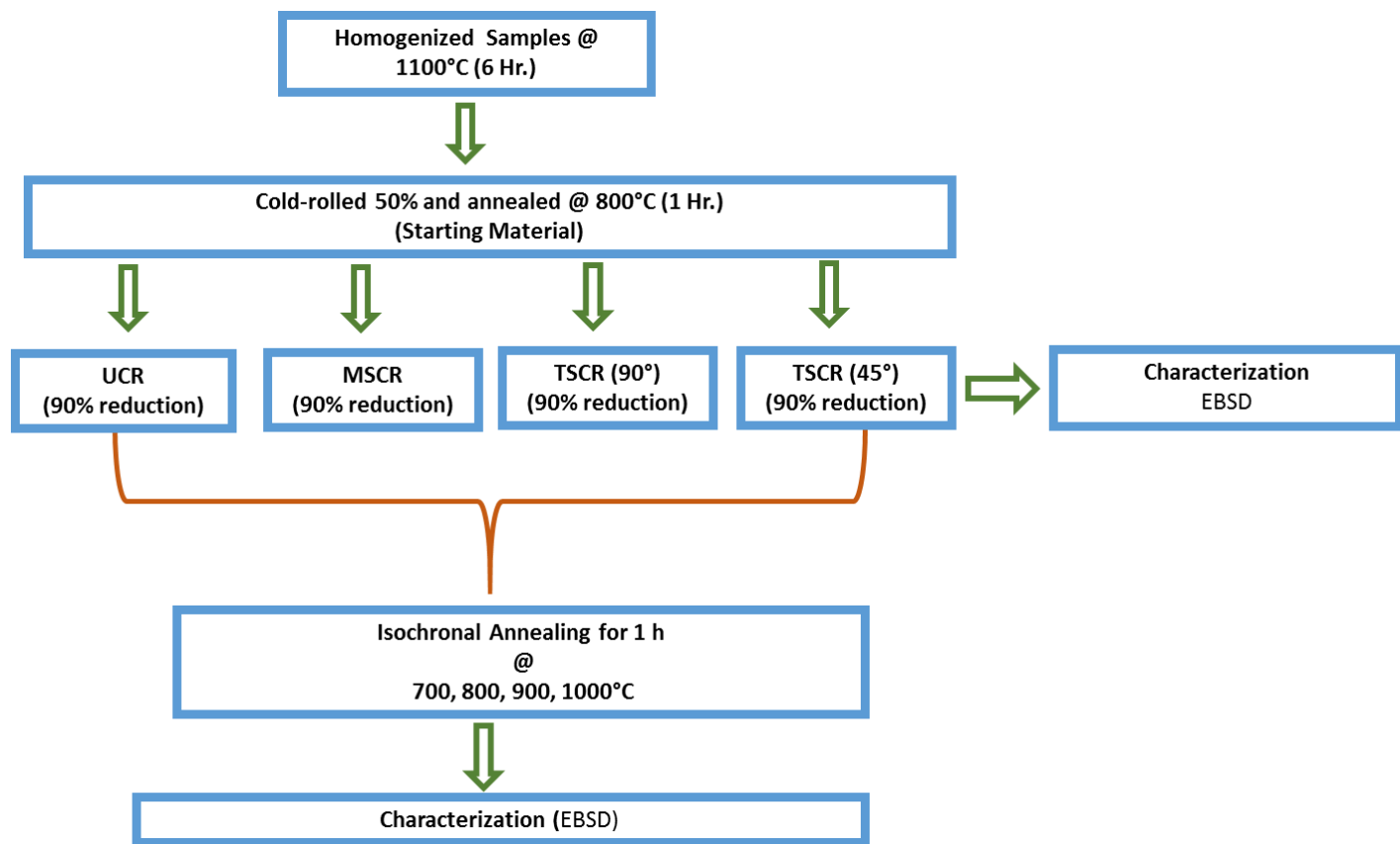


Fig 3.1: Experimental flow chart of the present work.

## 3.2 Processing

### 3.2.1 Cold-rolling

To achieve deformation using different strain paths, four different rolling routes were employed. However, the final thickness reduction was 90% (corresponding to a true strain ( $\epsilon$ ) = 2.65) in different cold-rolling routes. These routes are namely, UCR (Unidirectional Rolling), MSCR (Multi Step Cross Rolling), TSCR (90°) (Two Step Cross Rolling [90°]) and TSCR (45°) (Two Step Cross Rolling [45°]). In UCR route the samples were cold-rolled along a single direction. In other words, the rolling direction (RD) was unchanged. In the MSCR route, the samples were rotated by 90° along Normal Direction (ND) after each pass of  $\epsilon = 0.2$ , such that the Transverse Direction (TD) of previous pass is the RD of the next pass. In the TSCR (90°) route, the samples were deformed up to a true strain of  $\epsilon = 1.2$  (i.e. corresponding to a thickness reduction of 65%) in a single direction and then deformed till  $\epsilon = 2.65$  (i.e. corresponding to 90% reduction) after rotation of 90° about the ND. In TSCR (45°) route, the samples were deformed up to the true strain of  $\epsilon = 1.2$  in a single direction. Then the sheets were cut along 45° to the RD and further cold-rolled to  $\epsilon = 2.65$  (i.e. corresponding to 90% reduction) so that the new RD was at angle of 45° with respect to the previous RD. The different rolling routes are schematically shown in as shown in Fig.3.2

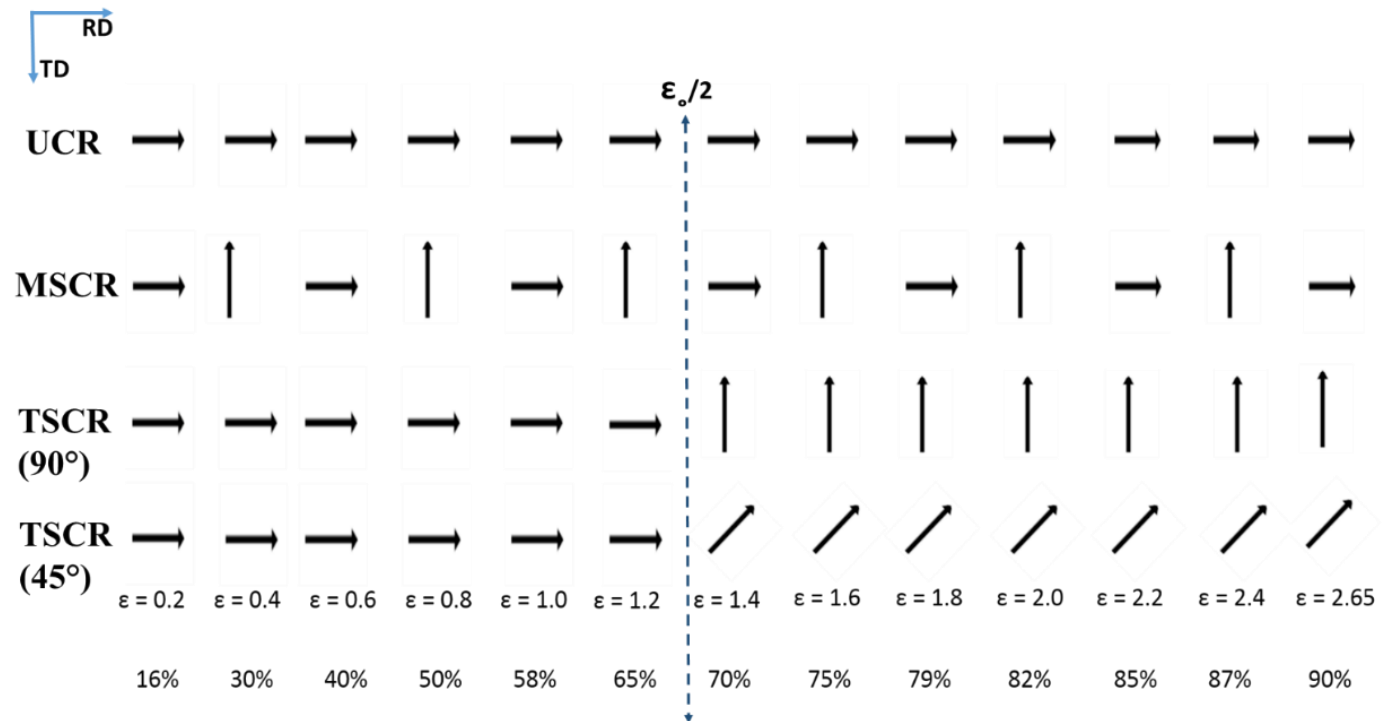


Fig.3.2: Schematic representation of different rolling routes (arrow represents the RD).

### **3.2.2 Annealing**

In order to understand the effect of strain path change on the evolution of recrystallization microstructure and texture, small samples obtained from the 90% cold-rolled sheets were subjected to isochronal annealing for 1 hour at temperatures varying from 700°C to 1000°C. These samples were quenched immediately in cold water following the recrystallization treatments.

### **3.3 Material Characterization**

The microstructure and texture of the cold rolled and annealed samples were characterized by using SEM-EBSD (Scanning Electron Microscopy-Based Electron Backscattered Diffraction). For EBSD investigation, the 90% rolled and annealed samples of all processing routes were carefully mechanical polished till 1  $\mu$  m using colloidal silica in an automatic polishing machine (Tegramin-25, Struers, Denmark). These samples were electro polished using the electrolyte of 90% methanol+ 10% perchloric acid at -5° C temperature using a constant voltage of 12-15 volts applied for 15 seconds.

An EBSD system (Oxford Instruments UK) attached to a Field Emission Gun type Scanning Electron Microscope (FEG-SEM, Carl Zeiss Germany model: SUPRA 40) was used to measure the microstructure and texture of the samples. The Aztech-HKL software (Oxford Instruments, UK) was used for data acquisition. The acquired EBSD data was exported to TSL-OIM™ software (EDAX Inc., USA) for analysis purpose. A cut off angle of 15° was used for calculating the volume fraction of individual texture components. The Orientation Distribution Functions (ODFs) were calculated using the series expansion method with series rank 22.

# Chapter 4: Results

## 4.1 Starting material

The Grain Boundary (GB) map obtained from the EBSD scan of the RD-ND section of the starting material is shown in Fig.4.1(a). The High Angle Grain boundaries (HAGBs) and the annealing twin boundaries ( $\Sigma 3$  defined by  $60^\circ\langle 111 \rangle$  relations) are indicated by the black and red lines, respectively. The GB map reveals that the starting material is fully recrystallized with an average grain size of  $\sim 7 \mu\text{m}$  (excluding the twin boundaries). Comparison of the (111) pole figure (PF) (Fig.4.1(b)) with that of the ideal (111) PF (Fig.4.1(c)) indicates the presence of a rather weak texture.

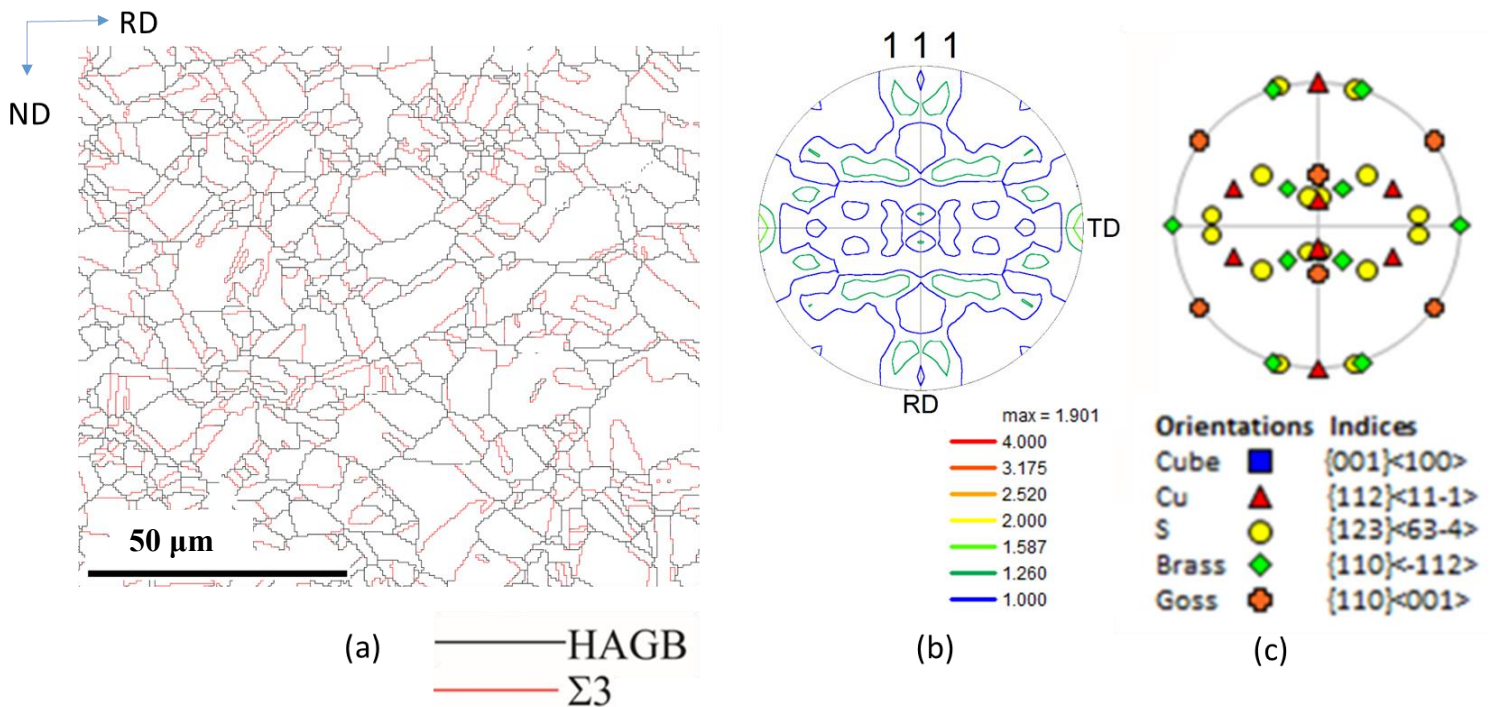


Fig. 4.1: (a) GB map and (b) (111) PF of the HEA prepared by 50% deformation and annealing at  $800^\circ\text{C}$  for 1 h of the homogenized alloy. (c) is the ideal (111) PF showing the locations of the important individual FCC texture components.

## 4.2 Deformation microstructure and texture

The microstructures of 90% deformed materials processed by the UCR (Fig.4.2(a)), MSCR (Fig.4.2(b)), TSCR (90°) (Fig.4.2(c)) and TSCR (45°) (Fig.4.2(d)) are shown by the image quality (IQ) maps in Fig.4.2. Fragmented microstructure with thin shear bands (indicated by arrows) running 25° to 35° to the RD are observed in the different 90% deformed materials. More lamellar structure as compared to the UCR processed material (Fig.4.2(a)) could be observed in the MSCR (Fig.4.2(b)) and TSCR (90°) (Fig.4.2(c)) processed materials. From the IQ map of the 90% deformed TSCR (45°) material (Fig.4.2(d)), the density of shear bands appears higher than other rolling routes.



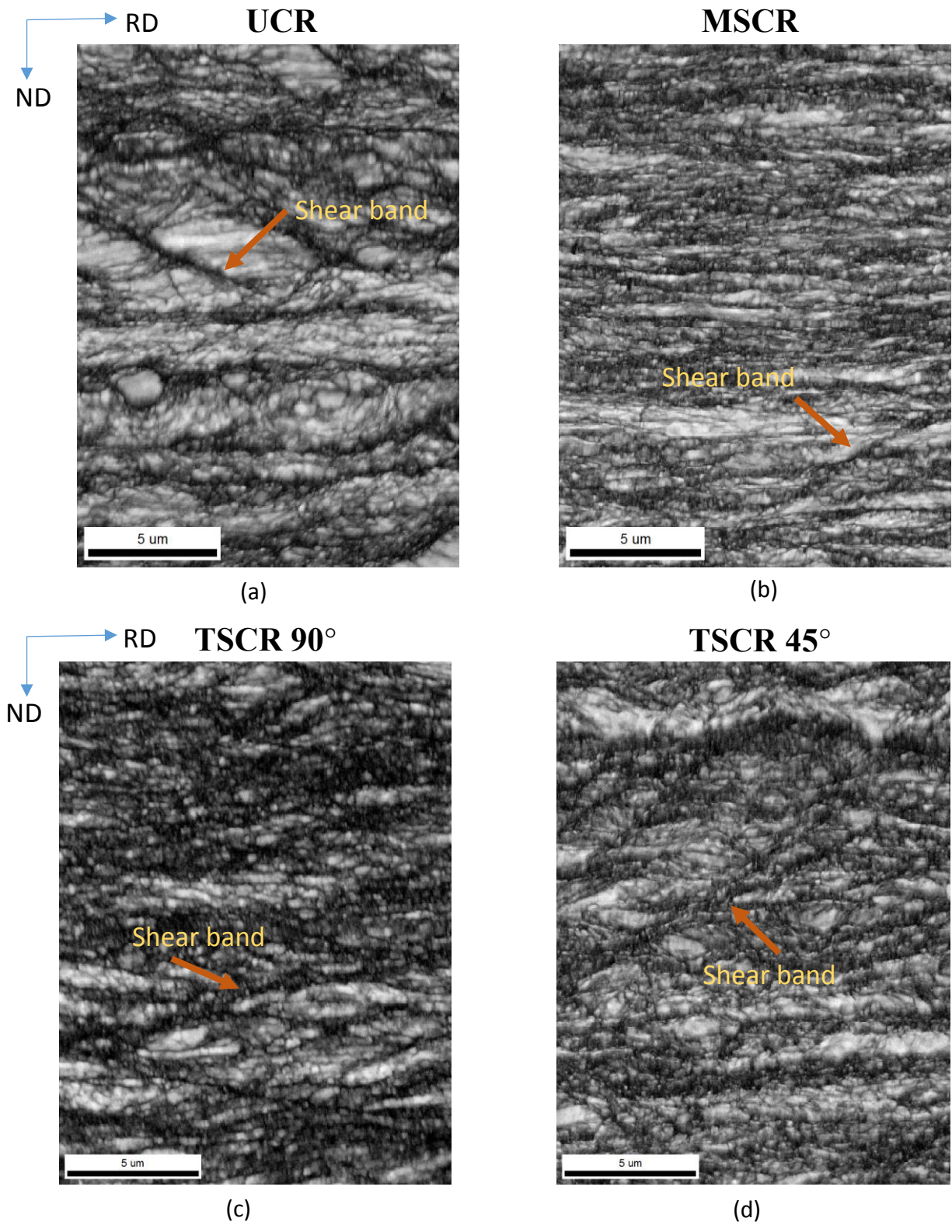












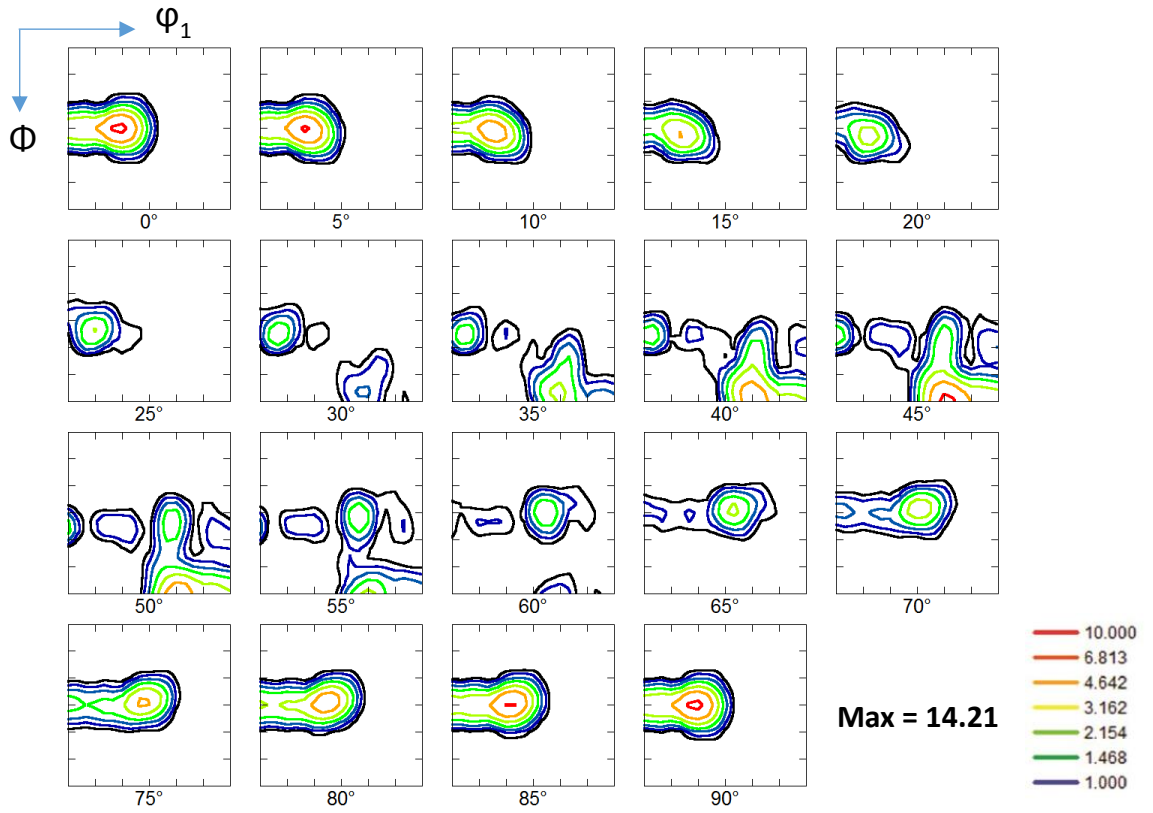


Fig. 4.2: IQ maps showing the microstructure of (a) UCR, (b) MSCR, (c) TSCR (90°) and (d) TSCR (45°) processed materials deformed to 90% reduction in thickness.

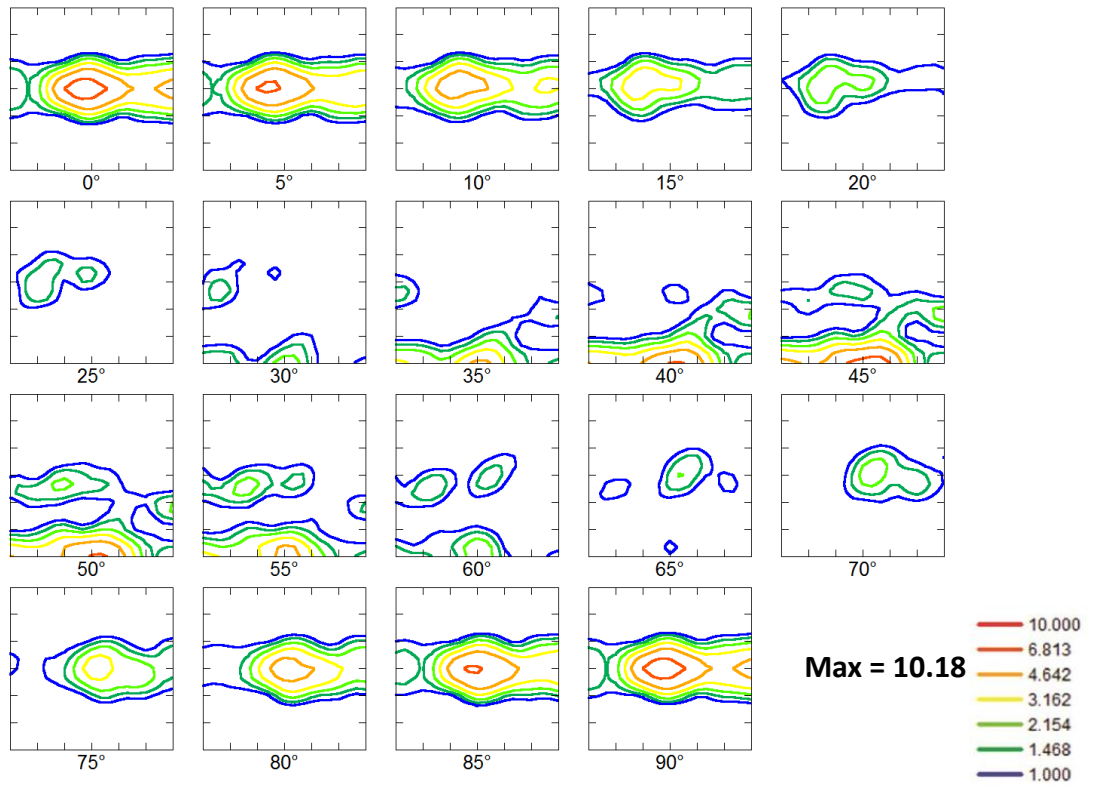
The textures of the 90% deformed materials processed by the UCR (Fig.4.3(a)), MSCR (Fig.4.3(b)), TSCR (90°) (Fig.4.3(c)) and TSCR (45°) (Fig.4.3(d)) are shown in Fig.4.3 by complete ODFs. The locations of the important ideal deformation and recrystallization texture components are summarized in Table 1. The UCR processed material shows the development of a strong Brass ( $B_S$ ) orientation  $\{110\} \langle 112 \rangle$  ( $\phi_1, \Phi, \phi_2 = 35^\circ, 45^\circ, 0^\circ$ ) along with G/B  $\{110\} \langle 115 \rangle$  ( $\phi_1, \Phi, \phi_2 = 17^\circ, 45^\circ, 0^\circ$ ) and S  $\{123\} \langle 634 \rangle$  ( $\phi_1, \Phi, \phi_2 = 59^\circ, 37^\circ, 63^\circ$ ) orientations.

Table 1: Important deformation and recrystallization texture components.

Texture Component		Symbol	Euler Angle (°)			Miller Indices
			$\Phi_1$	$\Phi$	$\Phi_2$	
Cube (C)			0	0	0	$\{001\} \langle 100 \rangle$
Copper (Cu)			90	35	45	$\{112\} \langle 111 \rangle$
S			59	37	63	$\{123\} \langle 634 \rangle$
Brass ( $B_S$ )			35	45	0	$\{110\} \langle 112 \rangle$
Goss (G)			0	45	0	$\{110\} \langle 001 \rangle$
Rt-G			90	45	0	$\{110\} \langle 110 \rangle$
G/B			17	45	0	$\{110\} \langle 5\ 5\ 23 \rangle$
$B_S^{ND}$	UCR, MSCR, TSCR(90°)		45	45	0	$\{110\} \langle 17\ 12\ 12 \rangle$
	TSCR(45°)		25	45	0	$\{110\} \langle 113 \rangle$
BR			80	31	34	$\{236\} \langle 385 \rangle$
D			90	25	45	$\{113\} \langle 332 \rangle$
K			27	64	14	$\{142\} \langle 211 \rangle$
M			80	30	65	$\{13\ 6\ 25\} \langle 20\ 15\ 14 \rangle$



(a)



(b)

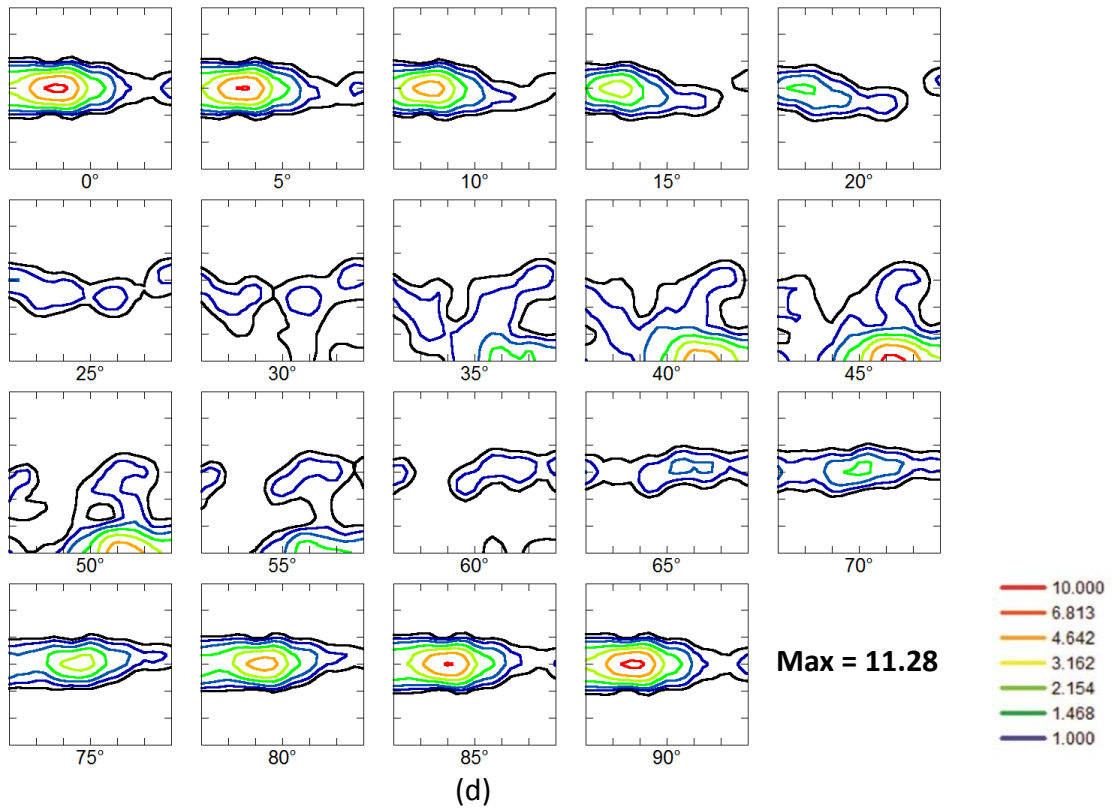
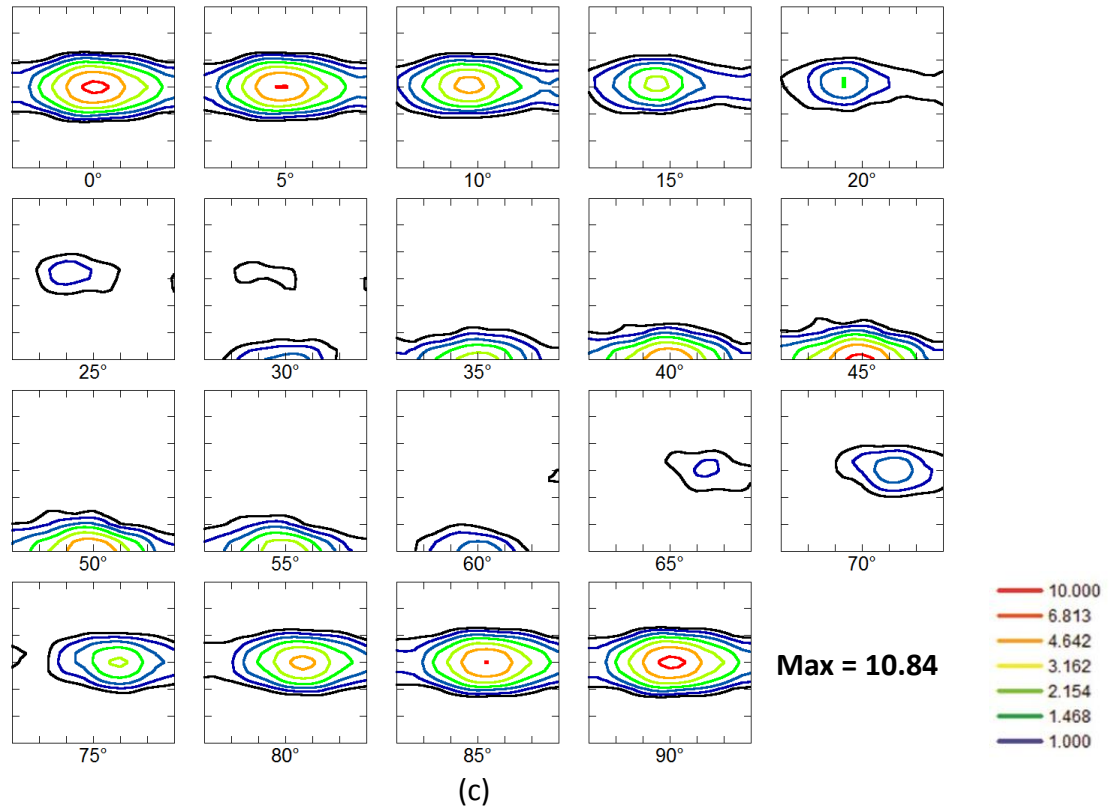


Fig.4.3: ODFs of (a) UCR, (b) MSCR, (c) TSCR (90°) and (d) TSCR (45°) processed materials deformed up to 90% reduction in thickness.

The maximum intensity along the  $\alpha$ -fiber for the MSCR route (Fig.4.3(b)) has been shifted from the ideal  $B_s$  location ( $\phi_1, \Phi, \phi_2 = 35^\circ, 45^\circ, 0^\circ$ ) to ( $\phi_1, \Phi, \phi_2 = 45^\circ, 45^\circ, 0^\circ$ ) location corresponding to the ND-rotated Brass orientation ( $B_s^{ND}$ )  $\{110\} \langle 17 -12 12 \rangle$ . Along with the  $B_s^{ND}$  orientation, other alpha fiber components for e.g.  $B_s$  and rotated-Goss (Rt-G) ( $\phi_1, \Phi, \phi_2 = 90^\circ, 45^\circ, 0^\circ$ )  $\{110\} \langle 110 \rangle$  are observed. The  $\phi_2 = 0^\circ$  sections of the ODFs of TSCR ( $90^\circ$ ) (Fig.4.3(c)) and TSCR ( $45^\circ$ ) (Fig.4.3(d)) also show the presence of alpha fiber components. The maximum intensity peaks are found to be located at the ( $\phi_1, \Phi, \phi_2 = 45^\circ, 45^\circ, 0^\circ$ ) and ( $\phi_1, \Phi, \phi_2 = 25^\circ, 45^\circ, 0^\circ$ ) in TSCR ( $90^\circ$ ) and TSCR ( $45^\circ$ ) processed materials, respectively. Therefore, it may be easily recognized that differently processed materials show alpha-fiber orientations. However, the main intensity peaks for MSCR and TSCR( $90^\circ$ ) routes are found almost at the identical location i.e. at ( $\phi_1, \Phi, \phi_2 = 45^\circ, 45^\circ, 0^\circ$ ) corresponding to  $\{110\} \langle 17 -12 12 \rangle$ , however for the TSCR( $45^\circ$ ) route the main intensity peak is located at ( $\phi_1, \Phi, \phi_2 = 25^\circ, 45^\circ, 0^\circ$ ) corresponding to  $\{011\} \langle 3 -1 1 \rangle$ .

The development of texture due to different processing routes can be further understood from the quantitative texture analysis shown in Fig.4.4. It is clearly evident that in the UCR processed material that the typical FCC rolling texture components i.e.  $B_s$  or  $S$  are stronger as compared to that in the materials fabricated by other processing routes. In contrast, the MSCR processed material shows significantly stronger  $B_s^{ND}$  component. Both TSCR ( $90^\circ$ ) and TSCR ( $45^\circ$ ) show comparable volume fractions of the individual texture components. The quantitative analysis plot (Fig.4.4) shows higher volume fractions of random components in TSCR( $90^\circ$ ) and TSCR( $45^\circ$ ) processed materials as compared to UCR and MSCR processed materials.

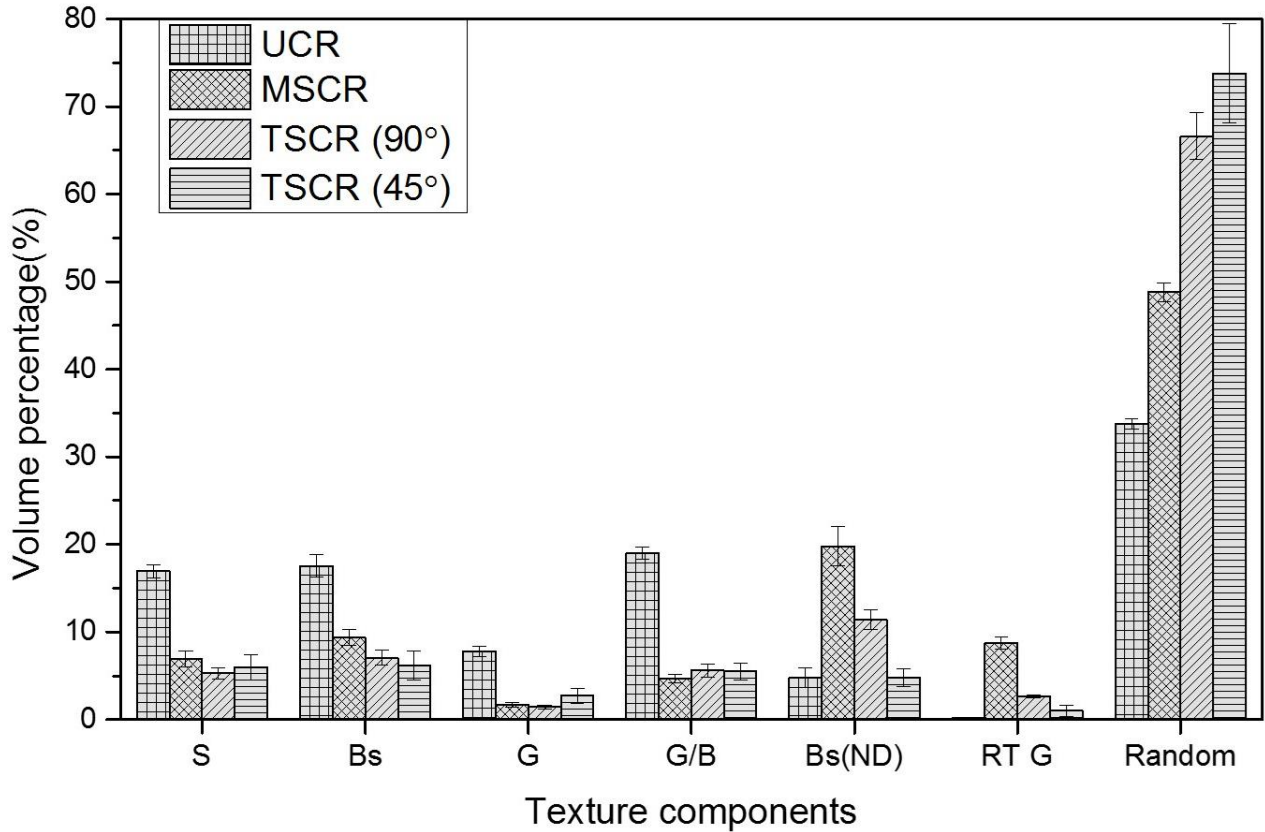


Fig 4.4: Quantitative texture representation by variation in volume percentage of individual texture components.

### 4.3 Microstructure and texture evolution of isochronal annealing

Fig.4.5 shows the development of microstructure following isochronal annealing of differently processed materials. Microstructure of the UCR processed material annealed at 700°C (Fig.4.5(a)) shows the development of a fully recrystallized fine microstructure with profuse annealing twins. Annealing at higher temperatures (Fig.4.5((b)-(c)) leads to grain growth. The annealed microstructures of the MSCR, TSCR(90°) and TSCR(45°) processed materials show very similar behavior.



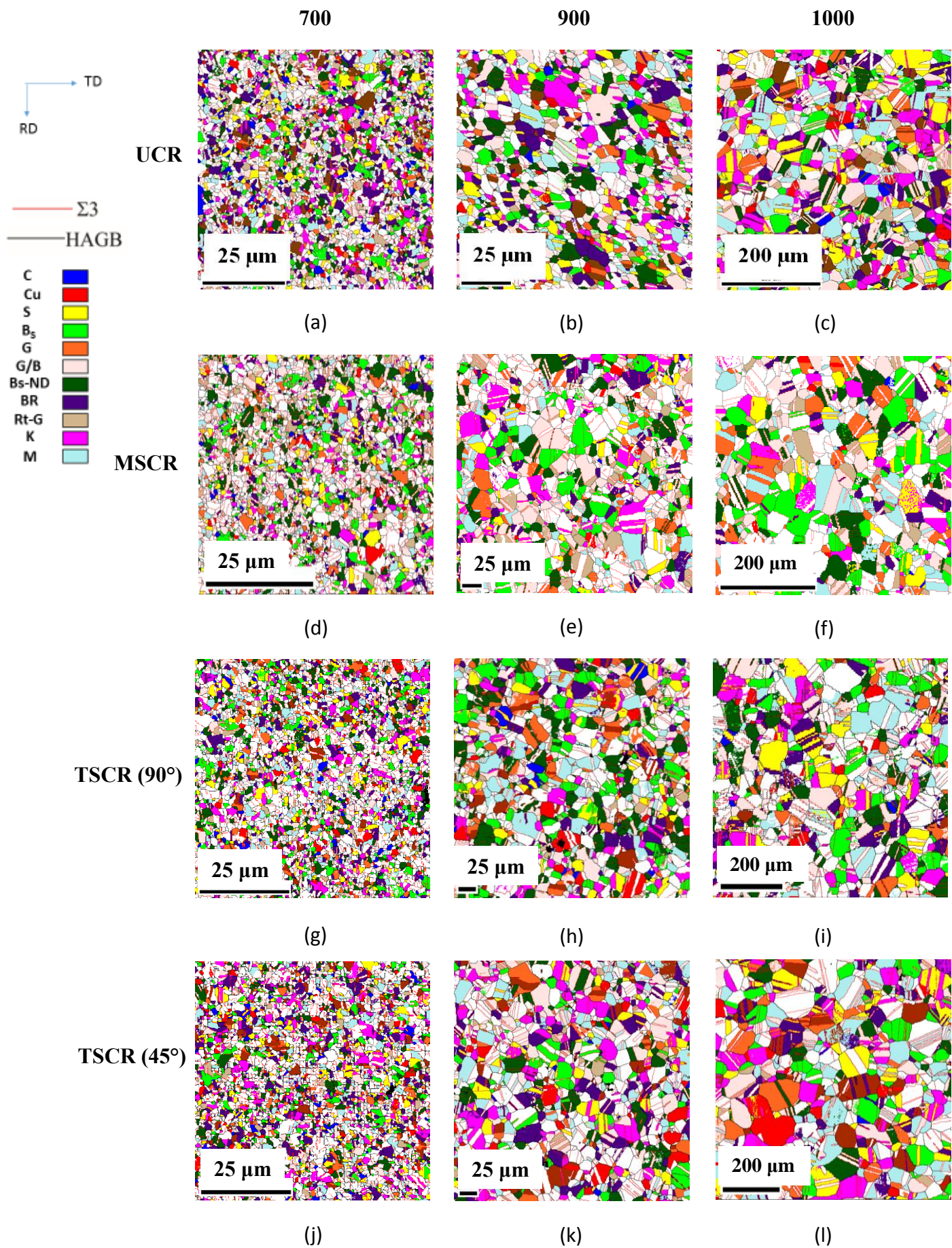
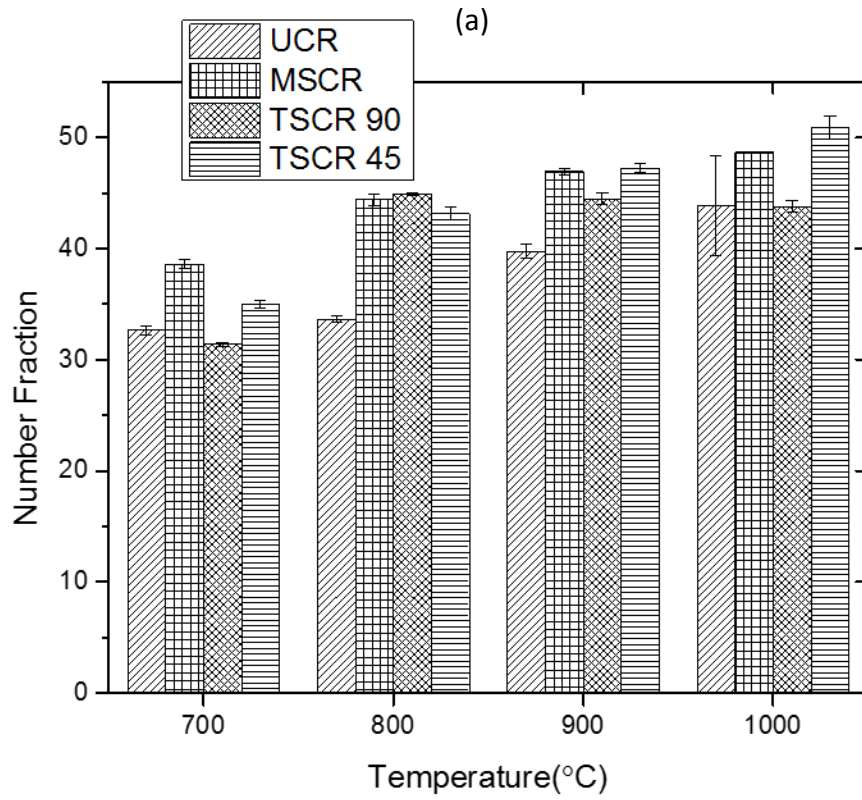
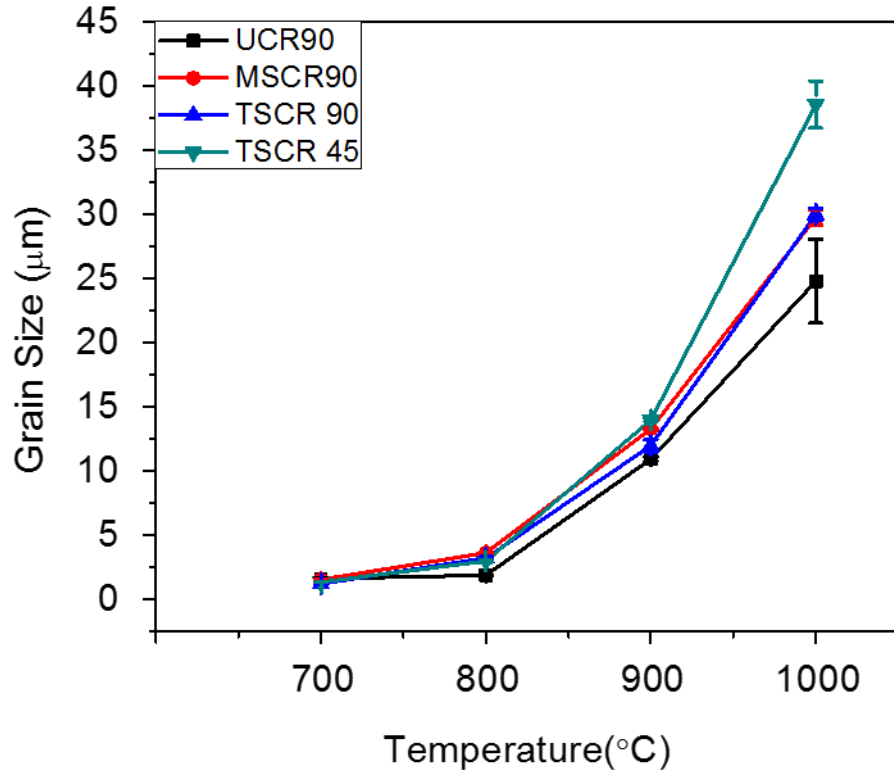


Fig 4.5: Orientation maps after annealing of 90% deformed materials processed by different routes.



(b)

Fig.4.6: Variation of (a) grain size (excluding twin boundaries) and (b)  $\Sigma 3$  twin boundary fraction with annealing temperature.



Fig 4.6 shows the evolution of key microstructural parameters, such as grain size (Fig.4.6(a)) and  $\Sigma 3$  twin boundary fraction (Fig.4.6(b)). The differences in the average grain size of differently processed materials ( $\leq 800^\circ\text{C}$ ) at lower annealing temperatures are not quite significant (Fig.4.6(a)). However, the grain size of the UCR processed material is certainly found to be the lowest. Annealing at higher temperatures results in significant differences in the average grain size of differently processed materials. It may be clearly seen that after annealing at  $1000^\circ\text{C}$ , the grain size of the UCR processed material is found to be the smallest ( $\sim 24 \mu\text{m}$ ) while that of the TSCR( $45^\circ$ ) is the largest ( $\sim 40 \mu\text{m}$ ). The average grain size of the MSCR and TSCR( $90^\circ$ ) processed samples are found to be quite similar ( $\sim 30 \mu\text{m}$ ). The fraction of twin boundaries is generally found to increase with increasing annealing temperature (Fig.4.6(b)).

In order to understand the evolution of recrystallization texture, the relevant sections of the ODFs of different annealed materials are examined carefully. The relevant ODF sections of ( $\phi_2 = 0^\circ, 15^\circ, 35^\circ, 45^\circ, 65^\circ$ ) UCR processed material following annealing at  $700^\circ\text{C}$  (Fig.4.7(a)),  $900^\circ\text{C}$  (Fig.4.7(b)) and  $1000^\circ\text{C}$  (Fig.4.7(c)). The UCR processed material shows the retention of discontinuous weak  $\alpha$ -fiber (Fig.4.7(a)) along with the presence of deformation texture components including S ( $\phi_1, \Phi, \phi_2 = 59^\circ, 37^\circ, 63^\circ$ ). The presence of the recrystallization texture component BR can also be noticed. In addition, appreciable intensity could also be observed at the vicinity of K ( $\phi_1, \Phi, \phi_2 = 27^\circ, 64^\circ, 14^\circ$ ) and M ( $\phi_1, \Phi, \phi_2 = 80^\circ, 30^\circ, 65^\circ$ ) orientations. The corresponding ODF sections do not show any appreciable differences with increasing annealing temperature. This indicates that the development of annealing texture is not significantly affected by the annealing temperature.

The MSCR (Fig.4.8), TSCR( $90^\circ$ ) (Fig.4.9) and TSCR( $45^\circ$ ) (Fig.4.10) processed materials show largely similar texture formation behavior as observed in case of the UCR processed material. A well-developed  $\alpha$ -fiber texture is observed in all cases after annealing at  $700^\circ\text{C}$  (Fig.4.8(a), Fig.4.9(a) and Fig.4.10(a)). The  $\alpha$ -fiber is retained even after annealing at higher temperatures (Fig.4.8((b)-(c)), Fig.4.9((b)-(c)), Fig.4.10((b)-(c))).

The variation of volume fractions of individual texture components with increasing annealing temperature can be observed from Fig.4.11. It is clearly observed for all the different cold-rolled materials that the volume fractions of different texture components only show rather marginal variations with annealing temperature.

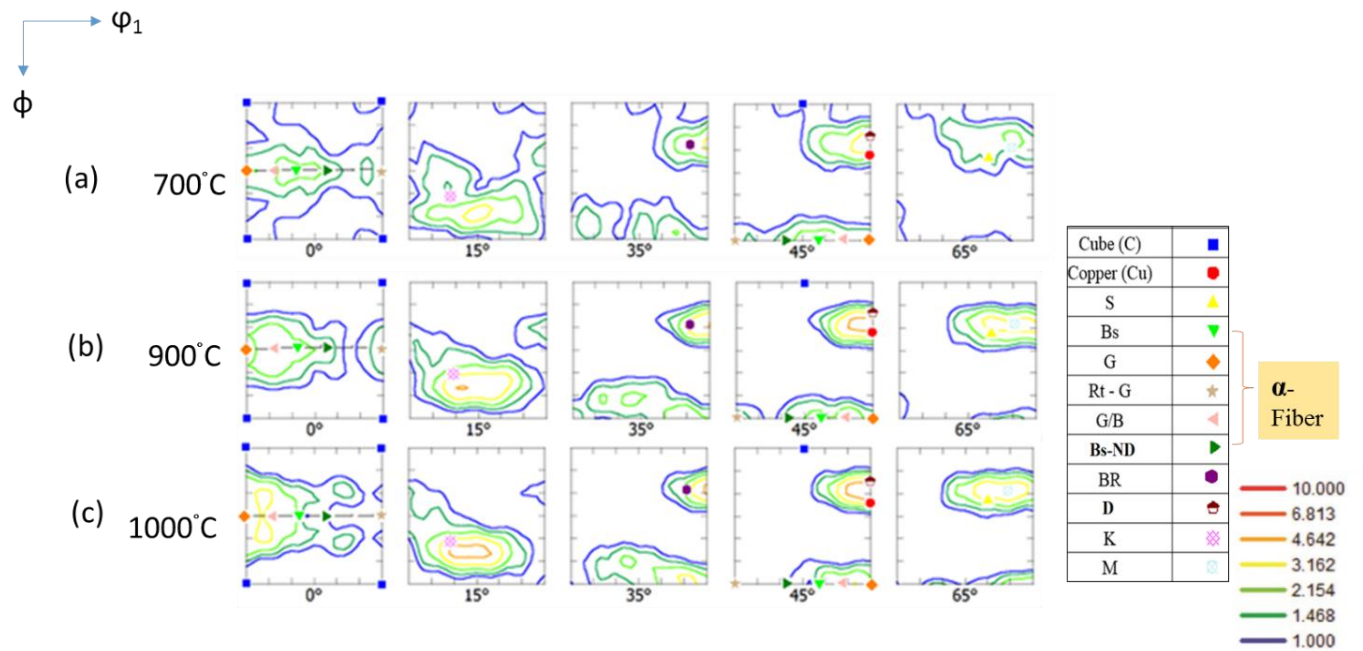


Fig. 4.7: Relevant ODF sections of the 90% UCR processed material annealed at (a) 700°C, (b) 900°C and (c) 1000°C for 1 hr.

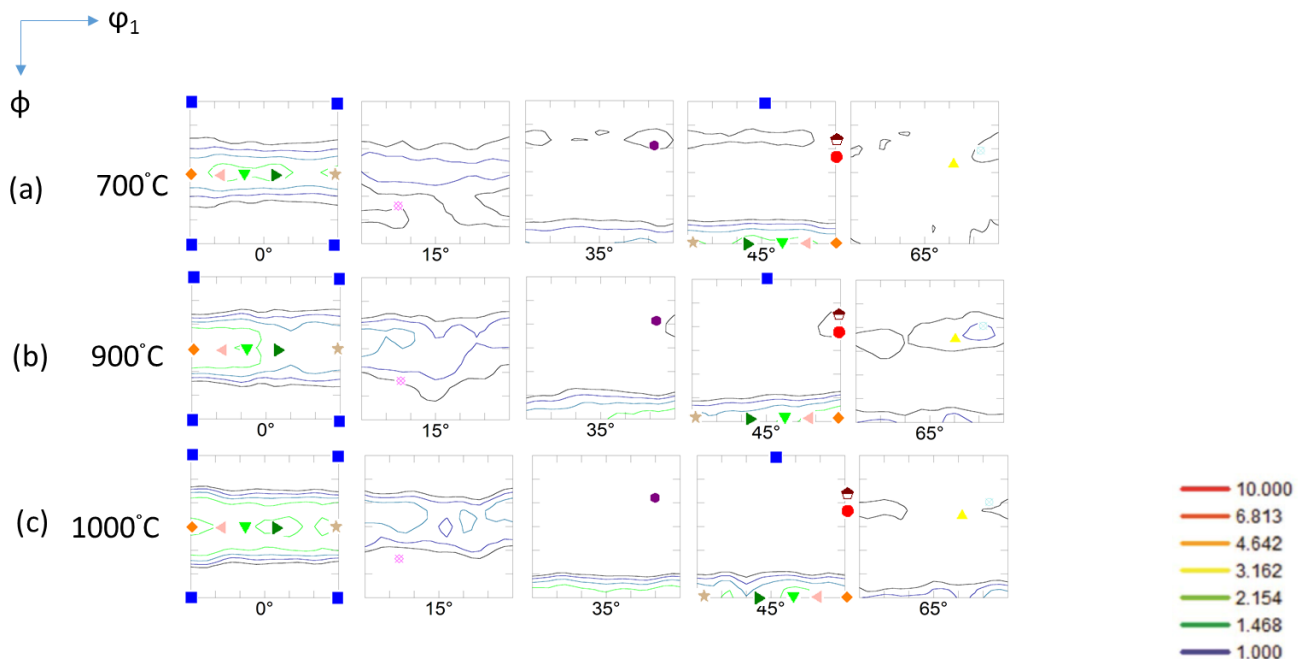


Fig. 4.8: Relevant ODF sections of the 90% MSCR processed material annealed at (a) 700°C, (b) 900°C and (c) 1000°C for 1 hr.

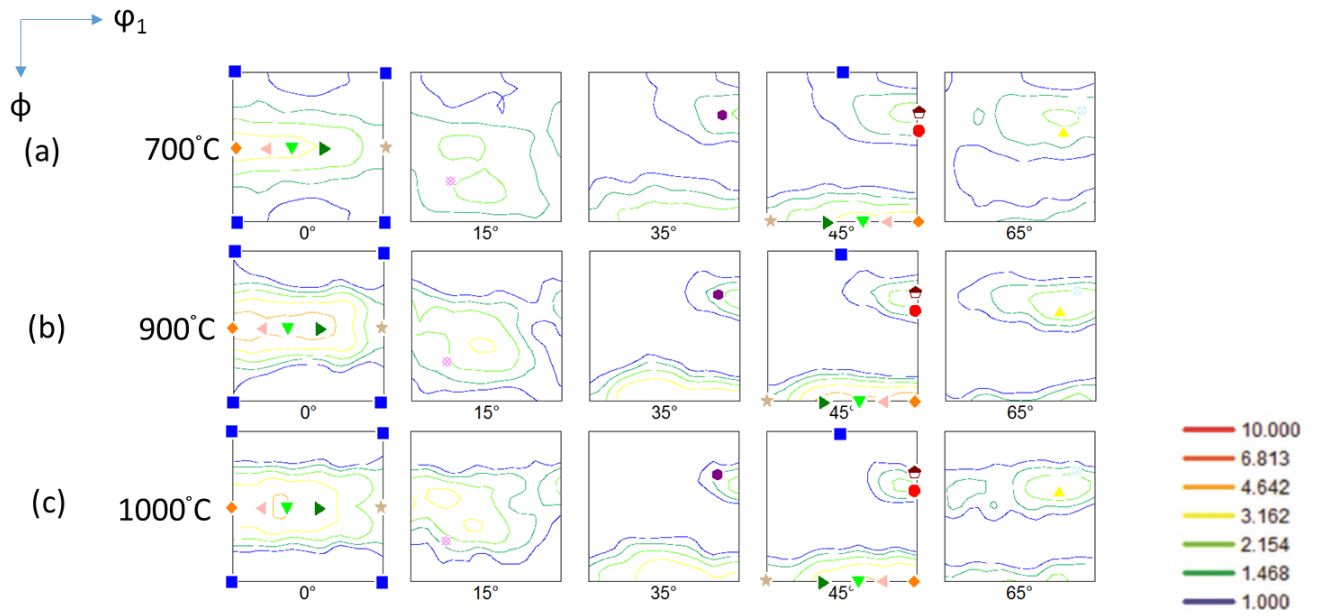


Fig. 4.9: Relevant ODF sections of the 90% TSCR (90°) processed material annealed at (a) 700°C, (b) 900°C and (c) 1000°C for 1 hr.

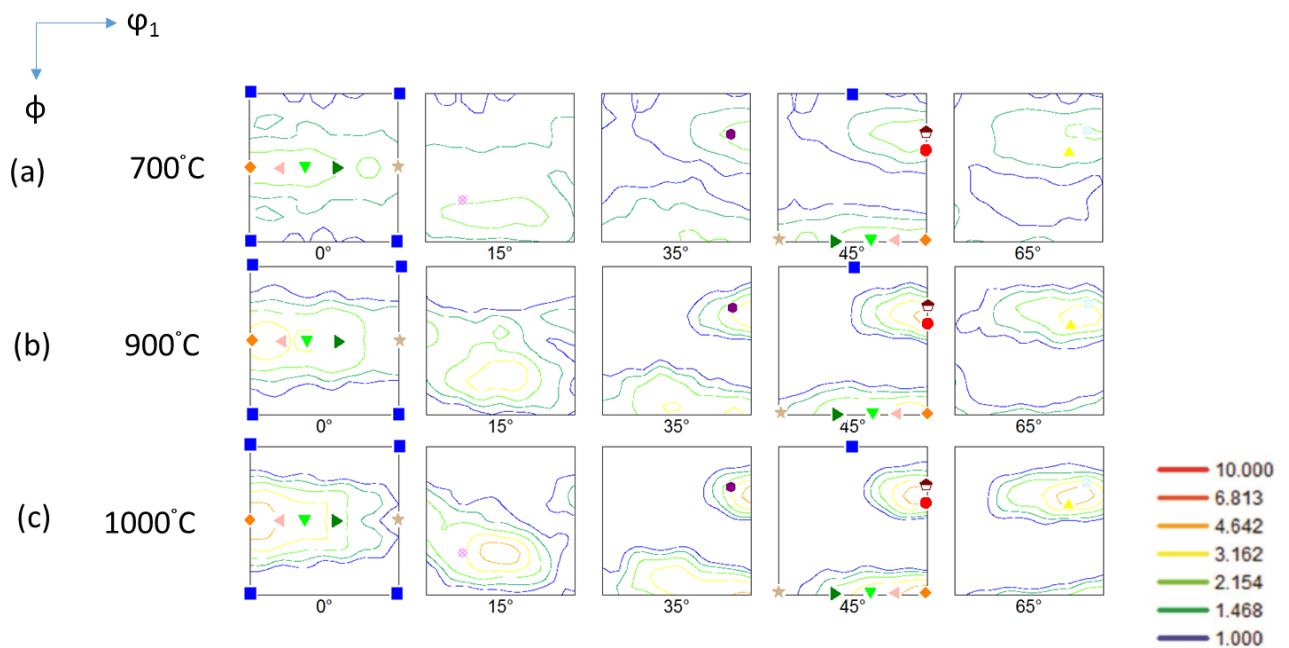
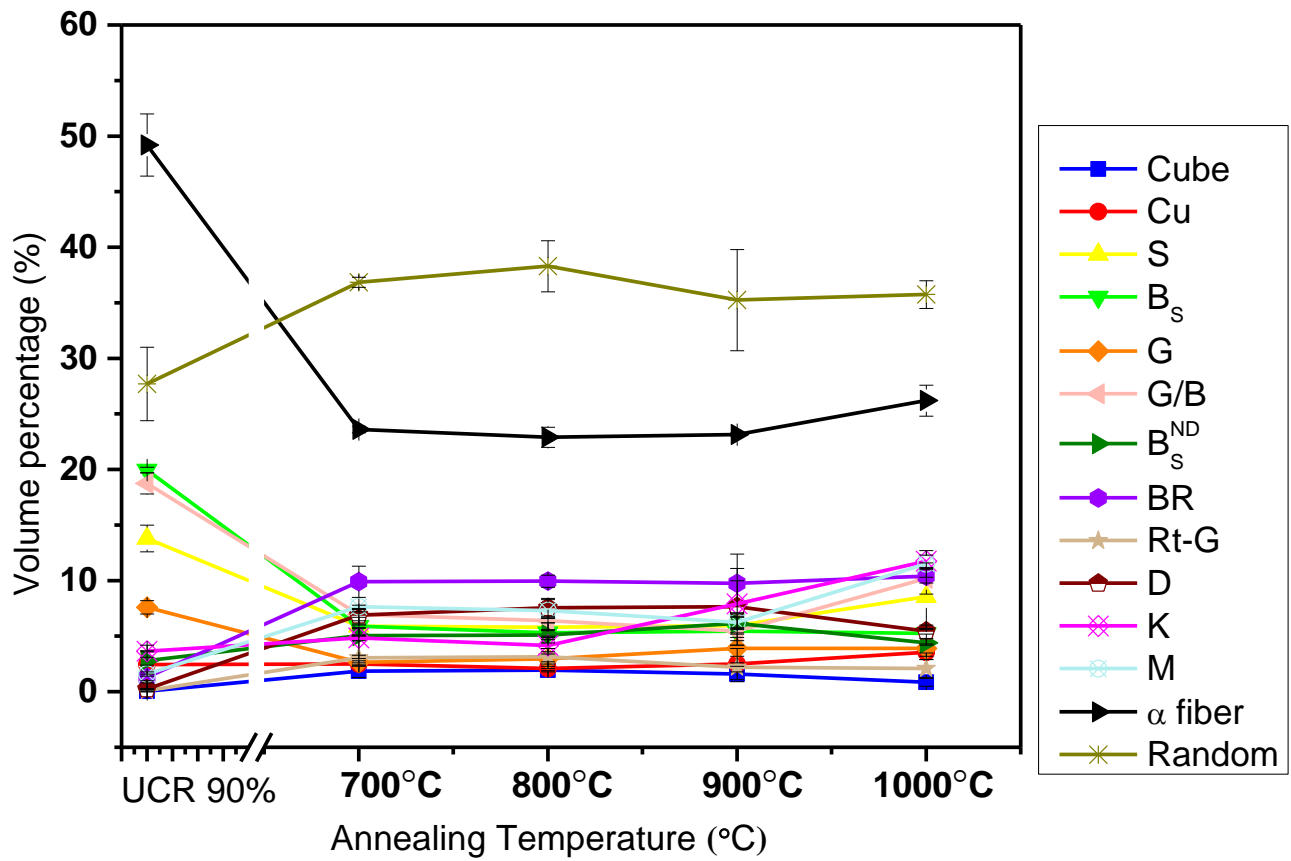
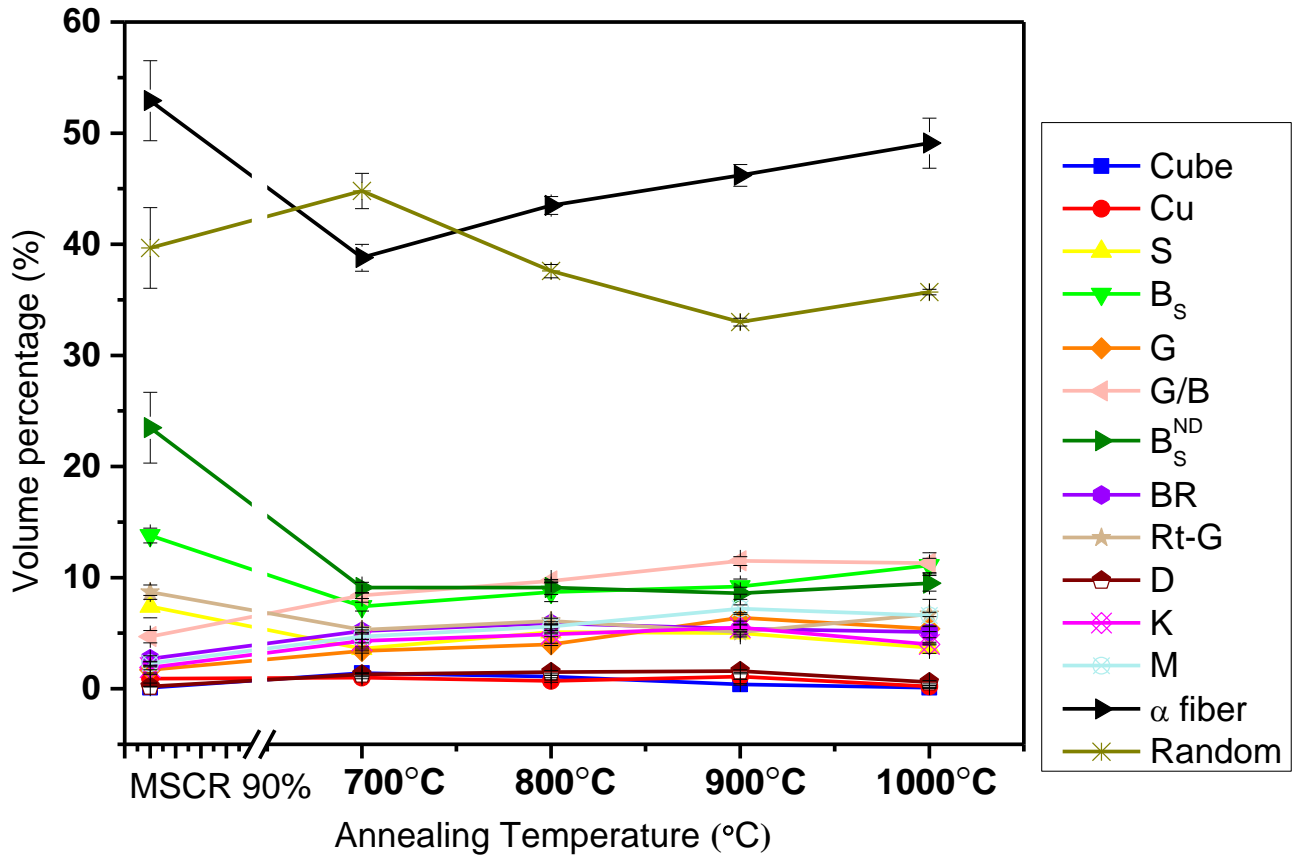


Fig. 4.10: Relevant ODF sections of the 90% TSCR (45°) processed material annealed at (a) 700°C, (b) 900°C and (c) 1000°C for 1 hr.



(a)



(b)

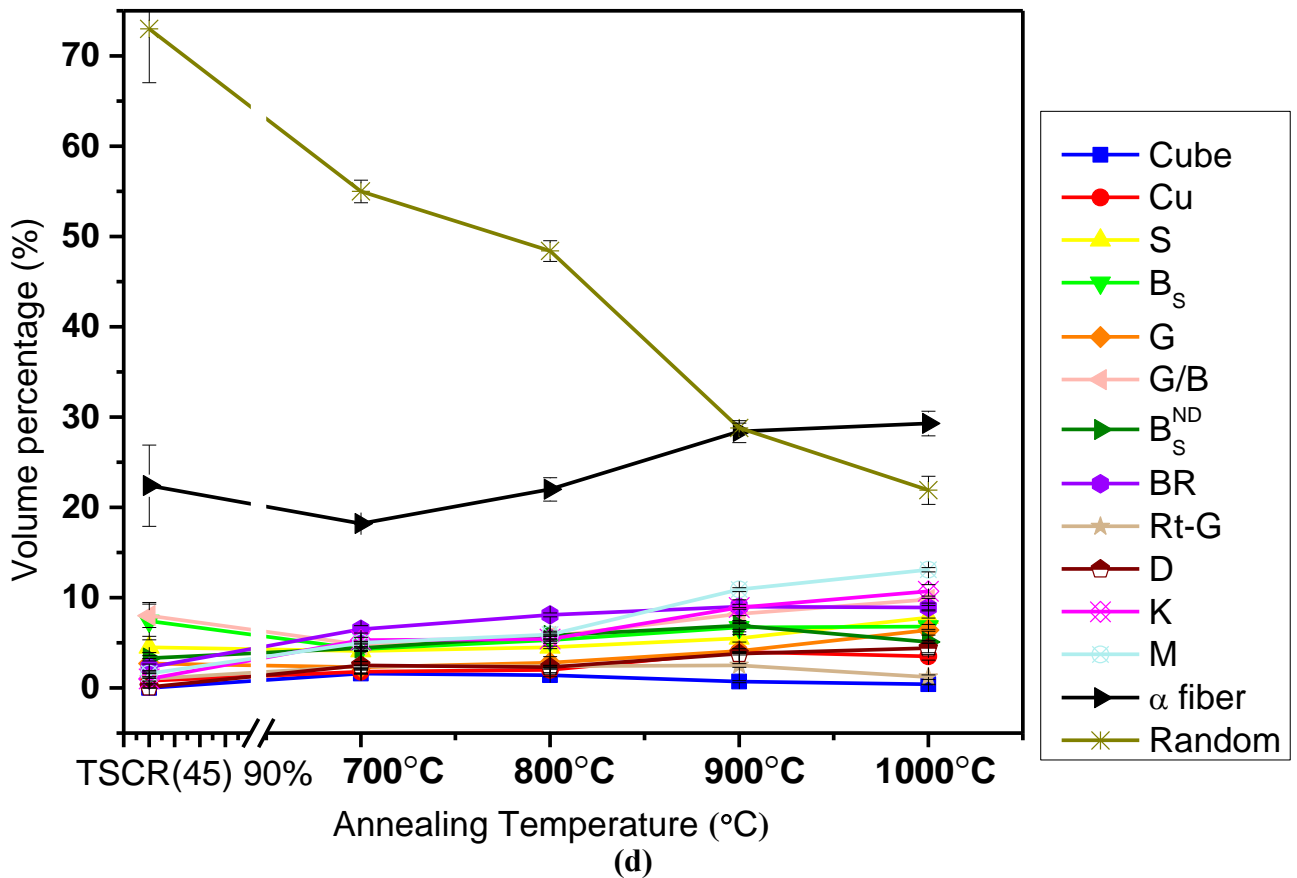
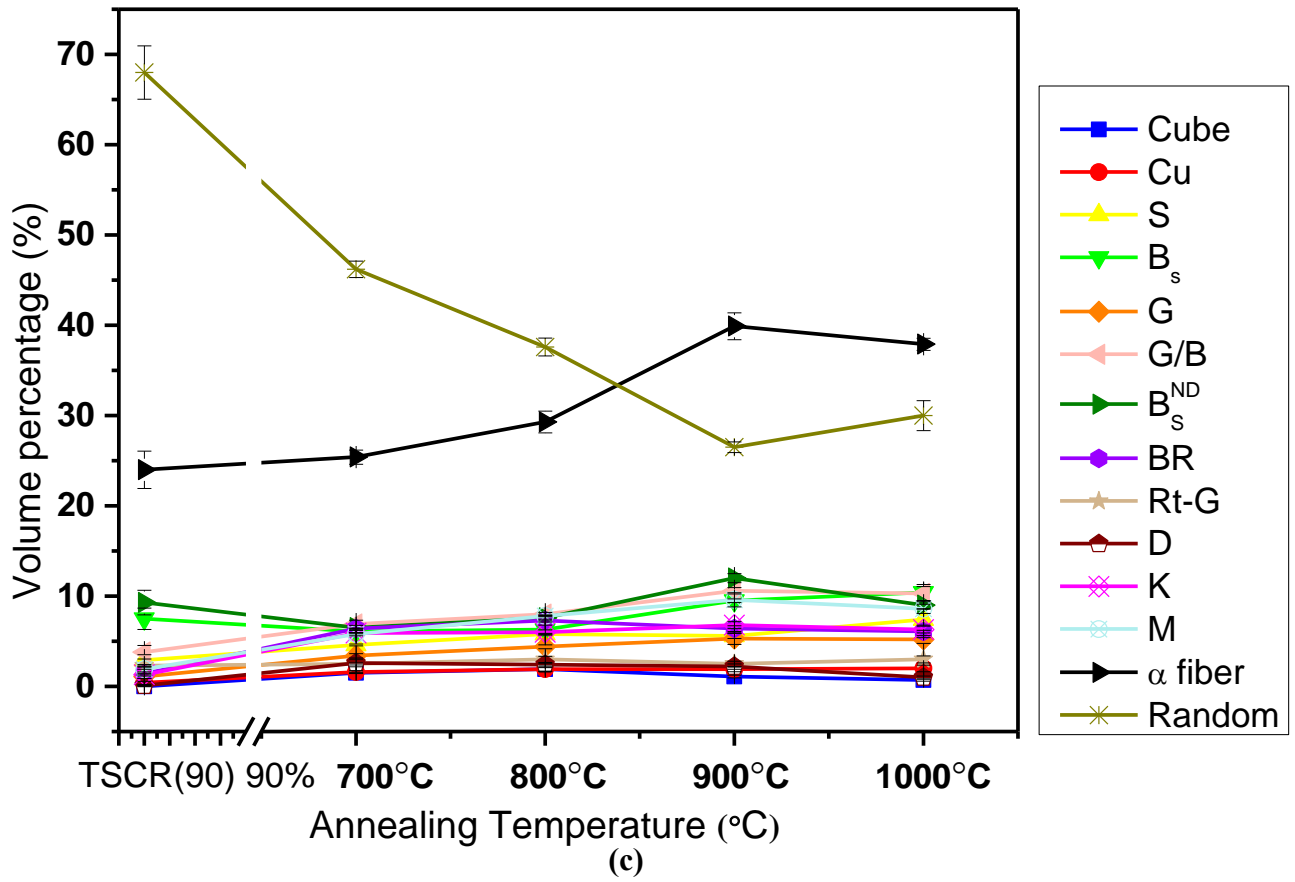


Fig.4.11: Variation of volume fraction of individual texture components with increasing temperature in (a) UCR, (b) MSCR, (c) TSCR (90°) and (d) TSCR (45°) deformed materials.

## Chapter 5: Discussion

The present work attempts to clarify the effect of strain path change during cold-rolling on the evolution of deformation and recrystallization texture in equiatomic CoCrFeMnNi HEA. For the sake of clarity, the deformation and annealing conditions will be discussed separately in the following sections.

### 5.1 Evolution of deformation microstructure and texture

The microstructure of the materials processed by the different rolling routes (Fig.4.2) reveal few common features, namely lamellar deformation structure, locally fragmented regions and presence of shear bands. The origin of the deformation induced lamellar microstructure subdivided by high angle grain boundaries (HABs) is attributed to the grain subdivision process [26, 27]. The grain subdivision process involves various microstructural mechanisms including formation of cell block structure dominated by long boundaries (microbands and dense dislocation walls), gradual increase in misorientation with increasing deformation due to the accumulation of dislocations, formation of shear bands at large strains resulting in large orientation gradient in a small volume, and finally coalescence of boundaries at large strains to form HABs [28, 29]. Further, grain orientation or texture can also play a significant role in the grain subdivision process. The relative rotation between different parts of a grain due to different slip activities can result in rotation to different end orientations [30].

In addition, the stacking fault energy (SFE) of materials also plays an important role during deformation. In low SFE materials, formation of deformation/mechanical twins emerges as an important mechanism in addition to the usual dislocation glide. It has been proposed that the TBs act as effective barriers to motion of dislocation. As a result, the glide dislocations are piled up against the TBs. The accumulation of dislocation at TBs gradually increases the misorientation, finally converting the TBs into new random HABs resulting in further refinement of microstructure [31]. The SFE of the present alloy is rather low  $\sim 18\text{-}20 \text{ mJ m}^{-2}$ . Thus, the observed ultrafine microstructure in different processed materials is consistent with the grain subdivision mechanism assisted by the low SFE of the alloy.

Gurao et al [20] have compared the microstructural development in Cu and Ni processed by different cross-rolling routes. These authors have found larger crystallite size in the UCR processed materials as compared to the different cross-rolling processed materials. This has been attributed to destabilization of substructure due to cross-rolling. While the formation of ultrafine microstructure in the present work can be well accounted for by the mechanism of grain subdivision, the precise grain size measurement could not be carried out. This should be a topic for future research.

The rolling texture of the UCR processed HEA is a predominantly brass or alloy type texture which is consistent with the low SFE of this alloy [32]. In contrast to the UCR processed material, the different cross-rolled materials show much lower volume fraction of the  $B_S$  component but increased volume fraction of the  $B_S^{ND}$  and random components. This implies that even though the SFE strongly affects the development of cold-rolling texture during uniaxial rolling (i.e. the UCR route), the development of deformation texture during cross-rolling is not strongly affected by the SFE. It might be noted that the development of  $B_S^{ND}$  dominated texture due to cross-rolling has been extensively reported in different medium to high FCC alloys. The development of deformation texture can be understood from the relative stability of different orientations during deformation. The stability of different orientations has been related to the rotation field  $\dot{R}$  ( $\phi_1, \phi, \phi_2$ ) and the divergence of the rotation field ( $div \dot{R} = \frac{\partial \phi_1}{\partial \phi_1} + \frac{\partial \phi}{\partial \phi} + \frac{\partial \phi_2}{\partial \phi_2}$ ) [33, 34]. For an orientation to be stable during deformation, two criteria given by,  $\dot{R} = 0$  and  $div(\dot{R}) = 0$ , need to be satisfied. Hong et al [19] have shown that amongst the different texture components, the orientation  $\{011\}\langle 1-11 \rangle$  (which is basically ND rotated  $B_S$  or  $B_S^{ND}$  orientation) would be stable under cross-rolling due to its higher inverse rotation rate and large negative divergence. As a result, the grains with orientations along the  $\alpha$ -fiber initially will rotate to the  $B_S$  orientation (which is the stable orientation during UCR) and then will further rotate away to the  $\{011\}\langle 1\bar{1}1 \rangle$  orientation when the RD is changed by  $90^\circ$  around the ND, thus, oscillating between the  $B_S$  and  $B_S^{ND}$  orientations, which would be the two dynamically stable end orientations in the cross rolled materials. Therefore, the orientations along the  $\alpha$ -fiber start converging at the middle of the two end orientations, resulting in the build-up of maximum intensity precisely at the location ( $45^\circ, 45^\circ, 0^\circ$ ). This theoretical calculations are supported by the experimental evidences where

strong presence of  $\{011\}\langle 755\rangle$  component is observed, characterized by the spread around this orientation due to the oscillation between the two predicted stable end orientations.

The different cross-rolled materials evidently show the presence of  $B_s^{ND}$  components. The deformation texture of MSCR and TSCR( $90^\circ$ ) processed materials show strong intensities at the ( $45^\circ, 45^\circ, 0^\circ$ ) location, which is in excellent agreement with the theoretical and experimental analyses of Hong et al [19]. However, in case of the TSCR( $45^\circ$ ) processed material, the strongest intensity is located at ( $25^\circ, 45^\circ, 0^\circ$ ).

## 5.2 Evolution of annealed microstructure and texture

The evolution of annealed grain size depends on the competing phenomena of nucleation and growth. The potential nucleation sites during recrystallization include grain boundaries and deformation heterogeneities such as shear bands or transition bands having large orientation gradient. Greater number of potential nucleation sites and restricted growth lead to a finer annealed grain size. Different parameters such as increasing deformation or lower starting grain size results in large number of potential nucleation sites. Consequently, the final annealed grain size decreases with increasing deformation, smaller starting grain size or increasing heating rate in conventional alloys. Sathiaraj et al [11] have confirmed very similar behavior in the equiatomic CoCrFeMnNi HEA. However, the effect of cross-rolling on the final annealed grain size has been hardly investigated even for conventional materials.

The most interesting effect of strain path is realized during the evolution of annealed microstructure. It is clearly observed that UCR processed material consistently shows lower average grain size as compared to other cross-rolled materials. The average grain size of the differently processed materials is quite similar at lower annealing temperatures (i.e.  $700^\circ\text{C}$ ), but considerable difference could be observed following annealing at  $1000^\circ\text{C}$ . At lower annealing temperature where the diffusion is very limited, the grain size in differently processed materials are found quite similar. However, annealing at higher temperature where recrystallization is followed by grain growth, the differences in nucleation behavior become quite apparent. Based on the preceding discussion, it appears that the density of potential nucleation sites is decidedly greater in the UCR processed material as compared to the different cross-rolled materials. This is consistent with development of finer microstructure in the UCR processed material as compared to different cross-rolled materials [20]. Further, continuous destabilization of substructure during



cross-rolling [20] inhibits large misorientation build up which is so crucial for nucleation of recrystallization [16].

Interestingly, the TSCR( $45^\circ$ ) processed material shows the largest annealed grain size amongst the differently processed materials. The average grain size in the TSCR( $45^\circ$ ) processed material after annealing at  $1000^\circ\text{C}$  is  $\sim 45\mu\text{m}$ , which is significantly greater than that of the UCR ( $\sim 25\mu\text{m}$ ), MSCR and TSCR( $90^\circ$ ) ( $\sim 30\mu\text{m}$ ) processed materials. It appears that the presence of intersecting shear bands further destroys the misorientation build up and potential nucleation environment in the TSCR( $45^\circ$ ) processed material as represented in fig.5.2.

Possible mechanism for greater nucleation density in UCR processed material

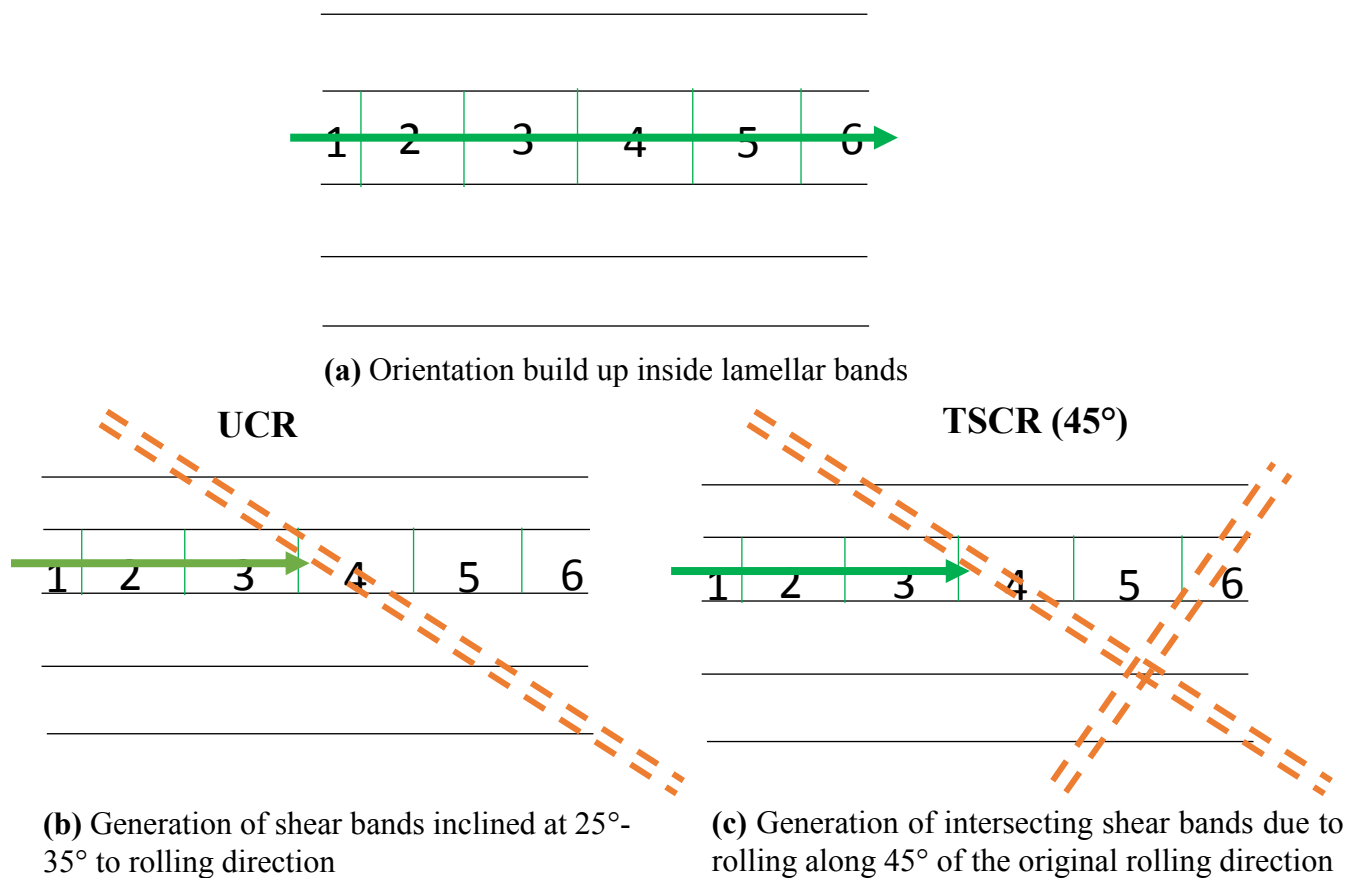


Fig. 5.1: Mechanism model for (a) representation of lamellar bands (b) representation of shear bands in UCR and (c) intersecting shear band structure in TSCR ( $45^\circ$ )

In spite of the observed differences in the deformation microstructure and texture, the differently processed materials show similarities in the development of deformation texture. The features of the recrystallization texture i.e. development of  $\alpha$ -fiber, retention and deformation texture components are observed in all the cases. Development of strong recrystallization texture, such as cube texture ( $\{001\}\langle 100\rangle$ ) in high to medium SFE alloys or BR ( $\{236\}\langle 385\rangle$ ) in low SFE alloys is usually associated with preferential nucleation or growth [16]. The absence of strong recrystallization texture in differently processed materials thus indicates the absence of strong preferential nucleation or growth in the present HEA which has also been reported earlier [11]. The insignificant change in the volume fractions of different texture components with annealing temperature is quite consistent with this behavior.

## Chapter 6: Summary and Conclusions

The main conclusions that may be drawn from the present study are:

1. Equiatomic CoCrFeMnNi has been successfully processed by UCR and different cross-rolling routes. Development of ultrafine microstructure and presence of shear bands could be observed in all the processed materials. This could be attributed to grain subdivision happening on an increasingly finer scale assisted further by the low SFE of the alloy.
2. UCR processed material develops a strong brass type texture in accordance with the low SFE of this alloy. The different cross-rolled materials show weaker  $B_S$  but stronger  $B_S^{ND}$  component. This could be attributed to strain path change which results in the convergence of orientations at the middle of the two end orientations during unidirectional and cross-rolling. While the main intensity peak in MSCR and TSCR(90°) is found very close to the predicted orientation, in case of the TSCR(45°) shift of the peak is observed.
3. The annealed grain size in the UCR processed materials is found to be but lower than other cross-rolled materials. The effect is much pronounced at higher annealing temperature where grain growth happens. This indicates greater density of potential nucleation sites in the UCR processed material as compared to others. Sluggish diffusion restricts grain growth so that the grain sizes appear similar after low temperature annealing.
4. Expected finer grain size in the UCR processed material provided greater density of nucleation sites. The destabilization of substructure during cross-rolling inhibits building of large misorientation crucial for nucleation of recrystallization. The largest grain size in the TSCR(45°) processed material appears to be due to propagation of intersecting shear bands which further destroys nucleation environment.

5. The recrystallization textures of different materials are characterized by the presence of  $\alpha$ -fiber and other retained deformation texture components. Absence of strong recrystallization texture could be attributed to the absence of strong preferential nucleation or growth.

## References

1. Yeh, J.W., et al., *Nanostructured High-Entropy Alloys with Multiple Principal Elements: Novel Alloy Design Concepts and Outcomes*. *Advanced Engineering Materials*, 2004. **6**(5): p. 299-303.
2. Yeh, J.-W., et al., *Formation of simple crystal structures in Cu-Co-Ni-Cr-Al-Fe-Ti-V alloys with multiprincipal metallic elements*. *Metallurgical and Materials Transactions A*, 2004. **35**(8): p. 2533-2536.
3. Zhang, Y., et al., *Microstructures and properties of high-entropy alloys*. *Progress in Materials Science*, 2014. **61**: p. 1-93.
4. Laktionova, M., et al., *Mechanical properties of the high-entropy alloy Ag<sub>0</sub>.<sub>5</sub>CoCrCuFeNi at temperatures of 4.2–300 K*. *Low Temperature Physics*, 2013. **39**(7): p. 630-632.
5. Yeh, J.-W., *Alloy design strategies and future trends in high-entropy alloys*. *Jom*, 2013. **65**(12): p. 1759-1771.
6. Tsai, K.-Y., M.-H. Tsai, and J.-W. Yeh, *Sluggish diffusion in Co–Cr–Fe–Mn–Ni high-entropy alloys*. *Acta Materialia*, 2013. **61**(13): p. 4887-4897.
7. Jien-Wei, Y., *Recent progress in high entropy alloys*. *Ann. Chim. Sci. Mat*, 2006. **31**(6): p. 633-648.
8. Otto, F., et al., *The influences of temperature and microstructure on the tensile properties of a CoCrFeMnNi high-entropy alloy*. *Acta Materialia*, 2013. **61**(15): p. 5743-5755.
9. Chuang, M.-H., et al., *Microstructure and wear behavior of Al<sub>x</sub>Co<sub>1.5</sub>CrFeNi<sub>1.5</sub>Ti<sub>y</sub> high-entropy alloys*. *Acta Materialia*, 2011. **59**(16): p. 6308-6317.
10. Murty, B., J.-W. Yeh, and S. Ranganathan, *High-entropy alloys*. 2014: Butterworth-Heinemann.
11. Bhattacharjee, P., et al., *Microstructure and texture evolution during annealing of equiatomic CoCrFeMnNi high-entropy alloy*. *Journal of Alloys and Compounds*, 2014. **587**: p. 544-552.

12. Sathiaraj, G.D. and P. Bhattacharjee, *Effect of cold-rolling strain on the evolution of annealing texture of equiatomic CoCrFeMnNi high entropy alloy*. Materials Characterization, 2015. **109**: p. 189-197.
13. Sathiaraj, G. and P. Bhattacharjee, *Effect of starting grain size on the evolution of microstructure and texture during thermo-mechanical processing of CoCrFeMnNi high entropy alloy*. Journal of Alloys and Compounds, 2015. **647**: p. 82-96.
14. Sathiaraj, G.D., et al., *Effect of heavy cryo-rolling on the evolution of microstructure and texture during annealing of equiatomic CoCrFeMnNi high entropy alloy*. Intermetallics, 2016. **69**: p. 1-9.
15. G.D. Sathiaraj, P.B., *Effect of heating rate on the evolution of microstructure and texture during annealing of heavily deformed equiatomic CoCrFeMnNi high entropy alloy*.
16. Rollett, A., et al., *Recrystallization and related annealing phenomena*. 2004: Elsevier.
17. Verlinden, B., et al., *Thermo-mechanical processing of metallic materials*. Vol. 11. 2007: Elsevier.
18. Hu, H. and R. Cline, *On the mechanism of texture transition in face centered cubic metals*. Texture, Stress, and Microstructure, 1988. **8**: p. 191-206.
19. Hong, S.-H. and D.N. Lee, *Deformation and recrystallization textures in cross-rolled copper sheet*. Journal of engineering materials and technology, 2002. **124**(1): p. 13-22.
20. Gurao, N., S. Sethuraman, and S. Suwas, *Effect of strain path change on the evolution of texture and microstructure during rolling of copper and nickel*. Materials Science and Engineering: A, 2011. **528**(25): p. 7739-7750.
21. Suwas, S. and A. Singh, *Role of strain path change in texture development*. Materials Science and Engineering: A, 2003. **356**(1): p. 368-371.
22. Bhattacharjee, P., et al., *The effect of starting grain size on the evolution of microstructure and texture in nickel during processing by cross-rolling*. Materials Characterization, 2013. **76**: p. 21-27.
23. Bhattacharjee, P., S. Saha, and J. Gatti, *Effect of Change in Strain Path During Cold Rolling on the Evolution of Microstructure and Texture in Al and Al-2.5% Mg*. Journal of materials engineering and performance, 2014. **23**(2): p. 458-468.

24. Zaid, M. and P. Bhattacharjee, *Electron backscatter diffraction study of deformation and recrystallization textures of individual phases in a cross-rolled duplex steel*. Materials Characterization, 2014. **96**: p. 263-272.
25. Bhattacharjee, P.P., et al., *Texture evolution during cross rolling and annealing of high-purity nickel*. Metallurgical and Materials Transactions A, 2013. **44**(6): p. 2707-2716.
26. Hansen, N. and D.J. Jensen, *Development of microstructure in FCC metals during cold work*. Philosophical Transactions of the Royal Society A: Mathematical, Physical and Engineering Sciences, 1999. **357**(1756): p. 1447-1469.
27. Godfrey, A. and D.A. Hughes, *Scaling of the spacing of deformation induced dislocation boundaries*. Acta Materialia, 2000. **48**(8): p. 1897-1905.
28. Hughes, D.A. and N. Hansen, *Microstructural evolution in nickel during rolling from intermediate to large strains*. Metallurgical Transactions A, 1993. **24**(9): p. 2022-2037.
29. Hansen, N., *Cold Deformation Microstructures*. Materials Science and Technology, 1990. **6**(11): p. 1039-1047.
30. Hughes, D.A. and N. Hansen, *High angle boundaries formed by grain subdivision mechanisms*. Acta Materialia, 1997. **45**(9): p. 3871-3886.
31. Wang, Y.B., et al., *The role of stacking faults and twin boundaries in grain refinement of a Cu-Zn alloy processed by high-pressure torsion*. Materials Science and Engineering: A, 2010. **527**(18-19): p. 4959-4966.
32. Leffers, T. and R.K. Ray, *The brass-type texture and its deviation from the copper-type texture*. Progress in Materials Science, 2009. **54**(3): p. 351-396.
33. Savoie, J. and J.J. Jonas, *Simulation of the deformation textures induced by deep drawing in extra low carbon steel sheets*. Acta Metallurgica Et Materialia, 1994. **42**(12): p. 4101-4116.
34. Toth, L.S., et al., *Development of Ferrite Rolling Textures in Low-Carbon and Extra Low-Carbon Steels*. Metallurgical Transactions a-Physical Metallurgy and Materials Science, 1990. **21**(11): p. 2985-3000.